

MIT Open Access Articles

*Prevention of tuberculosis in macaques
after intravenous BCG immunization*

The MIT Faculty has made this article openly available. **Please share**
how this access benefits you. Your story matters.

Citation: Darrah, Patricia A. et al. "Prevention of tuberculosis in macaques after intravenous BCG immunization." *Nature* 577, 7788 (January 2020): 95–102 © 2020 The Author(s)

As Published: <http://dx.doi.org/10.1038/S41586-019-1817-8>

Publisher: Springer Science and Business Media LLC

Persistent URL: <https://hdl.handle.net/1721.1/128216>

Version: Final published version: final published article, as it appeared in a journal, conference proceedings, or other formally published context

Terms of use: Creative Commons Attribution 4.0 International license



Prevention of tuberculosis in macaques after intravenous BCG immunization

<https://doi.org/10.1038/s41586-019-1817-8>

Received: 11 June 2019

Accepted: 11 November 2019

Published online: 1 January 2020

Open access

Patricia A. Darrah¹, Joseph J. Zeppa², Pauline Maiello², Joshua A. Hackney¹, Marc H. Wadsworth II^{3,4,5}, Travis K. Hughes^{3,4,5}, Supriya Pokkali¹, Phillip A. Swanson II¹, Nicole L. Grant⁶, Mark A. Rodgers², Megha Kamath¹, Chelsea M. Causgrove², Dominick J. Laddy⁷, Aurelio Bonavia⁷, Danilo Casimiro⁷, Philana Ling Lin⁸, Edwin Klein⁹, Alexander G. White², Charles A. Scanga², Alex K. Shalek^{3,4,5,10}, Mario Roederer^{1,11}, JoAnne L. Flynn^{2,11} & Robert A. Seder^{1,11*}

Mycobacterium tuberculosis (Mtb) is the leading cause of death from infection worldwide¹. The only available vaccine, BCG (Bacillus Calmette–Guérin), is given intradermally and has variable efficacy against pulmonary tuberculosis, the major cause of mortality and disease transmission^{1,2}. Here we show that intravenous administration of BCG profoundly alters the protective outcome of Mtb challenge in non-human primates (*Macaca mulatta*). Compared with intradermal or aerosol delivery, intravenous immunization induced substantially more antigen-responsive CD4 and CD8 T cell responses in blood, spleen, bronchoalveolar lavage and lung lymph nodes. Moreover, intravenous immunization induced a high frequency of antigen-responsive T cells across all lung parenchymal tissues. Six months after BCG vaccination, macaques were challenged with virulent Mtb. Notably, nine out of ten macaques that received intravenous BCG vaccination were highly protected, with six macaques showing no detectable levels of infection, as determined by positron emission tomography–computed tomography imaging, mycobacterial growth, pathology and granuloma formation. The finding that intravenous BCG prevents or substantially limits Mtb infection in highly susceptible rhesus macaques has important implications for vaccine delivery and clinical development, and provides a model for defining immune correlates and mechanisms of vaccine-elicited protection against tuberculosis.

Two billion people worldwide are infected with Mtb, with 10 million new cases of active tuberculosis (TB) and 1.7 million deaths each year¹. Prevention of pulmonary infection or disease in adolescents and adults would have the largest effect on the epidemic by controlling Mtb transmission³. The only licensed TB vaccine, BCG (live, attenuated *Mycobacterium bovis*), is administered intradermally at birth and provides protection against disseminated TB in infants but has variable efficacy against pulmonary disease in adolescents and adults².

T cell immunity is required to control Mtb infection and prevent clinical disease⁴. A major hurdle to developing an effective and durable T-cell-based vaccine against pulmonary TB is to induce and sustain T cell responses in the lung to immediately control infection while also eliciting a reservoir of systemic memory cells to replenish the lung tissue. Intradermal and intramuscular administration—the most common routes of vaccine administration—do not induce high frequencies of resident memory T (T_{RM}) cells in the lung. Studies performed 50 years ago suggested that administration of BCG by aerosol (AE) or

intravenous (IV) routes enhanced protection in non-human primates (NHPs) challenged shortly after immunization^{5–8}. However, there remains a limited understanding for mechanisms by which dose and route of BCG influence systemic and tissue-specific T cell immunity, and whether optimizing these variables would lead to high-level prevention of Mtb infection and disease. We hypothesized that a sufficiently high dose of IV BCG would elicit a high frequency of systemic and tissue resident T cells mediating durable protection against Mtb infection and disease in highly susceptible rhesus macaques.

Experimental design and safety

The central aim of this study was to assess how the route and dose of BCG vaccination influence systemic and tissue-resident T cell immunity, and protection after Mtb challenge. Rhesus macaques were vaccinated with 5×10^7 colony-forming units (CFUs) of BCG by intradermal (ID_{high}), AE or IV routes, or with a combination of both AE (5×10^7 CFUs) and ID

¹Vaccine Research Center, National Institute of Allergy and Infectious Diseases (NIAID), National Institutes of Health (NIH), Bethesda, MD, USA. ²Department of Microbiology and Molecular Genetics and Center for Vaccine Research, University of Pittsburgh School of Medicine, Pittsburgh, PA, USA. ³Ragon Institute of MGH, Harvard, and MIT, Cambridge, MA, USA. ⁴Department of Chemistry, Institute for Medical Engineering and Sciences (IMES), MIT, Cambridge, MA, USA. ⁵Broad Institute of MIT and Harvard, Cambridge, MA, USA. ⁶Department of Infectious Diseases and Microbiology, University of Pittsburgh School of Public Health, Pittsburgh, PA, USA. ⁷Aeras, Rockville, MD, USA. ⁸Department of Pediatrics, Children's Hospital of the University of Pittsburgh of UPMC, Pittsburgh, PA, USA. ⁹Division of Animal Laboratory Resources, University of Pittsburgh School of Medicine, Pittsburgh, PA, USA. ¹⁰Koch Institute for Integrative Cancer Research, MIT, Cambridge, MA, USA. ¹¹These authors contributed equally: Mario Roederer, JoAnne L. Flynn, Robert A. Seder. *e-mail: rseder@mail.nih.gov

(5×10^5 CFUs; AE/ID) (Extended Data Fig. 1a). Immune responses and protective efficacy of these regimens were compared to the standard human dose given ID (5×10^5 CFUs; ID_{low}). The dose of BCG selected for AE and IV vaccine groups was based on pilot dose-ranging studies (Supplementary Data 1). After BCG vaccination, immune responses in blood and bronchoalveolar lavage (BAL) were assessed over 24 weeks, after which NHPs were challenged with a low dose of Mtb (Extended Data Fig. 1b). Other macaques in each group were euthanized 1 or 6 months after vaccination for immune analysis of tissue responses (Extended Data Fig. 1c). To assess safety of BCG vaccinations, several clinical parameters were measured and found to be transiently affected by only IV BCG (Extended Data Fig. 2). A summary of all NHPs in this study and doses of BCG and Mtb administered are provided in Extended Data Fig. 1c and Supplementary Table 1.

Cellular composition of BAL and blood

Because generating immune responses in the lung was a major focus of the study, we first assessed whether the BCG vaccination regimen altered the number or composition of leukocytes in the BAL. Only IV BCG vaccination elicited significant changes in BAL cell numbers: a 5–10-fold increase in total cells, accounted for largely by conventional T cells (Fig. 1a and Supplementary Data 2a, b). This resulted in a sustained inversion of the alveolar macrophage:T-cell ratio up to 6 months after IV BCG vaccination (Extended Data Fig. 3a). Non-classical T cells (MAIT and V γ 9 γ 8) that can contribute to protection against TB^{9–11} were transiently increased 2–4 weeks after IV BCG (Fig. 1a, Extended Data Fig. 3b and Supplementary Data 2b). A similar analysis performed on peripheral blood mononuclear cells (PBMCs) showed no significant changes in leukocyte composition (Extended Data Fig. 3c, d). Neither BAL nor PBMCs exhibited changes in the proportion of natural killer cells, which were recently suggested to correlate with protection^{12,13} (Extended Data Fig. 3a, c). Finally, there were no increases in cytokines associated with trained innate immunity^{14,15} in stimulated PBMCs after ID or IV BCG immunization (Supplementary Data 3). Overall, these data show that IV BCG immunization, in contrast to AE or ID, results in significant and sustained recruitment of T cells to the airways and substantially alters the ratio of T cells to macrophages.

Antigen-responsive adaptive immunity

We next evaluated how these regimens influenced the ability of T cells responsive to mycobacterial antigen (such as purified protein derivative (PPD)) to produce the canonical cytokines (IFN γ , IL-2, TNF or IL-17) that are important for protection against TB^{4,16,17}. At the peak of the PBMC response (week 4), cytokine-producing CD4 T cells were higher in NHPs immunized with ID_{high} or IV BCG compared with those immunized with ID_{low} BCG; these responses declined over time but remained increased at week 24 (time of challenge; Fig. 1b and Extended Data Fig. 4a, g). PBMC CD8 responses in IV-immunized NHPs were greater than ID_{low} NHPs at both time points (Fig. 1c and Extended Data Fig. 4b, h). In BAL, antigen-responsive T cells peaked at 8 weeks and were largely maintained until time of challenge (Fig. 1d, e and Extended Data Fig. 4c, d). Compared with ID_{low} BCG, ID_{high} or AE BCG immunization elicited tenfold more PPD-responding CD4 T cells in BAL; IV BCG elicited 100-fold more PPD-responsive CD4 T cells, with approximately 40% of cells responding (Fig. 1d). Furthermore, only IV BCG induced an increase in antigen-responsive CD8 T cells (Fig. 1e). Central memory and transitional memory (T_{TM}) T cells¹⁸ comprised the majority of CD4 T cell responses in PBMCs across all vaccine groups at the peak of the response, whereas T_{TM} cells predominated in the BAL (Extended Data Fig. 4e, f). IV-BCG-vaccinated NHPs had the largest proportion of T_{TM} cells in PBMCs and effector memory (T_{EM}) cells in BAL.

Despite differences in the magnitude of T cell responses among vaccine regimens, there were no differences in the quality of T cell

responses (that is, the proportion of cells producing each combination of IFN γ , IL-2, TNF and IL-17)^{19,20} in PBMCs (Extended Data Fig. 5a and Supplementary Data 4) or the BAL (Extended Data Fig. 5b and Supplementary Data 5). Of the CD4 T cell responses, 90% consisted of T helper 1 (T_{H1}) cytokines, with fewer than 10% also producing IL-17; most IL-17-producing CD4 T cells co-expressed T_{H1} cytokines (Extended Data Fig. 5). Notably, approximately 10% of antigen-responsive CD4 T cells in PBMCs expressed CD154²¹ but no T_{H1} or T_{H17} cytokines (Extended Data Fig. 5a and Supplementary Data 4), which suggests that there may be underlying qualitative differences among vaccine group responses that are not measured by the canonical T cell cytokines commonly used to assess BCG-elicited immunity^{22,23}.

To expand the qualitative analysis of BAL T cell responses using an orthogonal approach, we performed single-cell mRNA sequencing (scRNA-seq) with Seq-Well²⁴ to comprehensively assess phenotypic and transcriptional states among T cells that might underlie protective vaccine responses (Fig. 1f–h, Extended Data Fig. 6 and Supplementary Data 6). We examined correlated patterns of gene expression within unstimulated and PPD-stimulated T cells from BAL to identify groups of genes for which the coordinated activity differed by regimen (Extended Data Fig. 6b). A total of seven significant T cell modules were identified among in vitro-stimulated T cells 13 weeks after immunization (Supplementary Table 2) and used to generate expression scores across all T cells at weeks 13 and 25. Among these, we identified a stimulation-inducible module of gene expression, module 2, enriched for memory T cell functionality (Supplementary Table 3 and Methods), primarily expressed in a population of BAL CD4 T cells from IV-BCG-immunized NHPs at week 13, and maintained until week 25 (Fig. 1f, g, Extended Data Fig. 6c, d and Supplementary Table 2). Differential gene expression analysis, comparing T cells positive and negative for module 2 (Fig. 1h and Supplementary Table 4), showed enrichment of genes previously associated with protection against TB including *IFNG*, *TBX21*, *RORC*, *TNFSF8*²⁵ and *IL21R*²⁶.

To further analyse adaptive immunity, we found that IV BCG elicited higher antibody responses in the BAL and plasma than the other routes. Mtb-specific IgG, IgA and IgM peaked 4 weeks after IV BCG vaccination and returned to baseline by 24 weeks in the BAL (Extended Data Fig. 7).

M. tuberculosis challenge outcome

Six months after BCG immunization, NHPs were challenged in three separate cohorts with a nominal dose of 10 CFUs of the highly pathogenic Mtb Erdman strain, with a pre-defined study end point of 12 weeks after challenge (Extended Data Fig. 1b, c and Supplementary Table 1). Infection and disease were tracked serially using ¹⁸F-fluorodeoxyglucose (FDG) positron emission tomography–computed tomography (PET–CT) imaging. Total FDG activity in lungs, a measure of cellular metabolism that correlates with total thoracic mycobacterial burden^{27,28}, was negative in all immunized macaques before Mtb challenge, but was increased throughout infection in unvaccinated NHPs (Fig. 2a). Three-dimensional reconstructions of pre-necropsy PET–CT scans are shown in Fig. 2b. All ID_{low} and AE-BCG-immunized NHPs had increased FDG activity in lungs over 12 weeks. Two NHPs in the ID_{high} and AE/ID BCG groups had no lung FDG activity and two NHPs in the ID_{high} group had inflammation at 8 weeks that returned to baseline by 12 weeks, suggesting partial protection. By contrast, nine out of ten IV-BCG-immunized NHPs had no lung FDG activity throughout the challenge phase (Fisher's exact test, $P < 10^{-4}$ compared to ID_{low} BCG) (Fig. 2a–c).

PET–CT was used to track granuloma formation after Mtb infection as a correlate of active disease²⁷. By 4 weeks and throughout infection, granulomas were detected in all unvaccinated as well as ID_{low}, ID_{high}, AE- and AE/ID-BCG-immunized NHPs (Fig. 2a). By contrast, IV-BCG-immunized NHPs had fewer granulomas compared with the benchmark ID_{low} BCG regimen ($P < 0.001$), with six out of ten NHPs having no granulomas throughout infection (Fig. 2a, d). Detailed necropsies

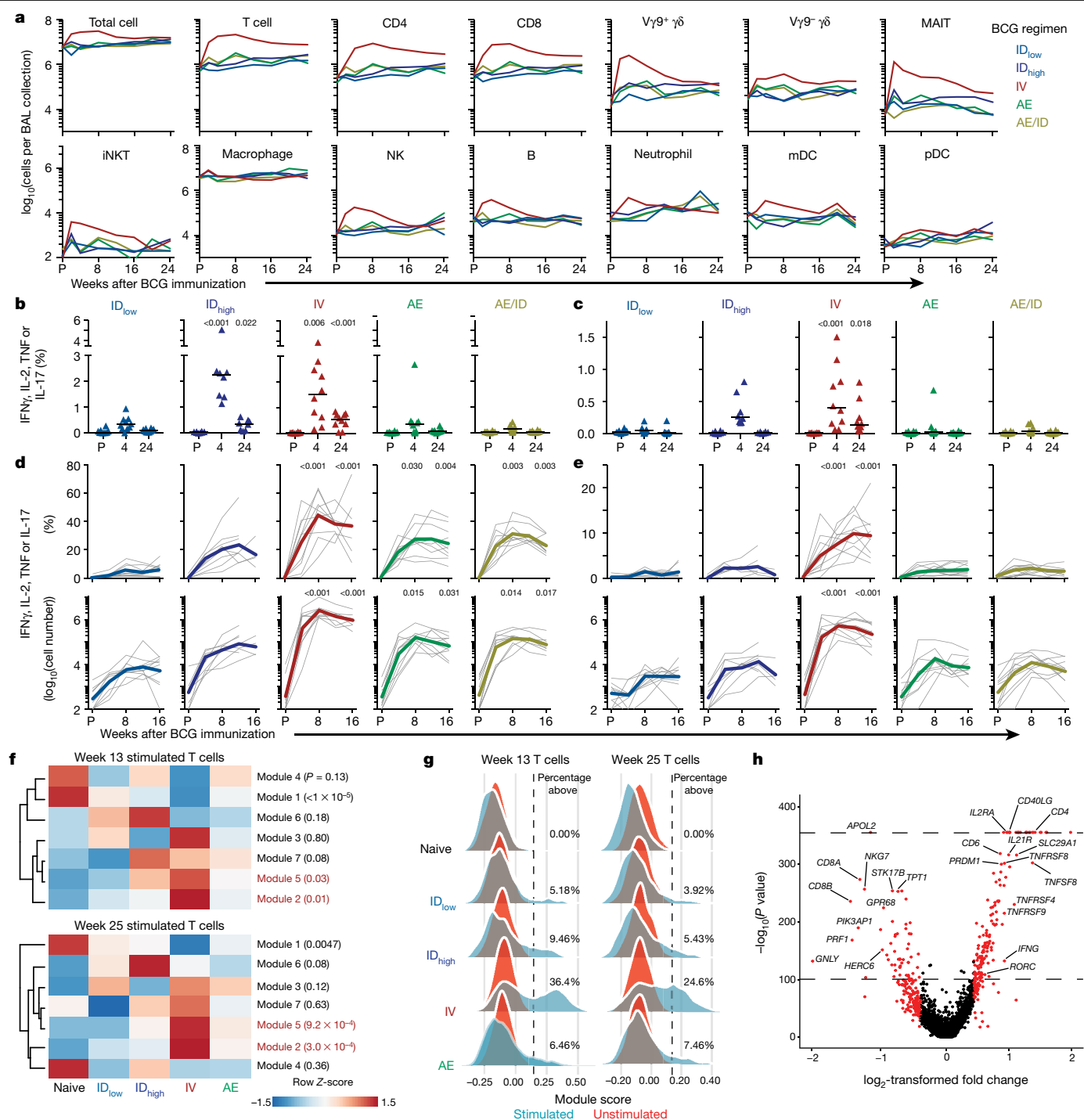


Fig. 1 | Cellular composition and immune analysis in blood and BAL after BCG vaccination. **a**, Number of cells (geometric mean) per BAL collection for leukocyte populations in each vaccine group before (pre, P) and up to 24 weeks after BCG; Supplementary Data 2 shows individual NHPs and statistical comparisons. Data are from cohorts 1–4 ($n = 11$ –13 macaques per group as outlined in Extended Data Fig. 1) except at weeks 2, 20 and 24 (cohort 4 only, $n = 3$). $V\gamma 9^{+/-}$, $V\gamma 9^{+/-} \gamma\delta$ T cells; MAIT, mucosal-associated invariant T cells; mDC, myeloid dendritic cells; NK, natural killer cells; iNKT, invariant natural killer cells; pDC, plasmacytoid dendritic cells. **b**, **c**, Percentage of memory CD4 (**b**) or CD8 (**c**) T cells in PBMCs producing IFN γ , IL-2, TNF or IL-17 after PPD stimulation in vitro. Shown are individual and median (horizontal bar) responses for NHPs in challenge study (cohorts 1–3, $n = 8$ –10 macaques) at weeks 4 (peak) and 24 (time of challenge) after BCG vaccination. **d**, **e**, Percentage (top) and number (bottom) of cytokine $^{+}$ memory CD4 (**d**) and CD8 (**e**) T cells in the BAL before and up to 16 weeks after BCG vaccination. Shown are individual (grey lines) and

mean (coloured lines) responses for challenge cohorts ($n = 8$ –10 macaques). Each group was compared to ID_{low} at weeks 4 and 24 for PBMCs (one-way ANOVA; P values are Dunnett's multiple comparison test) or weeks 8 and 16 for BAL (Kruskal–Wallis test; P values are Dunn's multiple comparison test). **f–h**, Single-cell transcriptional analysis of BAL cells at weeks 13 and 25 after BCG vaccination (cohort 4; $n = 3$ per group). **f**, Z-scored heat maps of the average cellular score for modules identified in week 13 PPD-stimulated T cells at weeks 13 and 25 after BCG vaccination. Red P values indicate modules uniquely elevated in the IV BCG group (one-way ANOVA). **g**, Distributions of module 2 expression in unstimulated and stimulated T cells at weeks 13 and 25 for each group. Percentage module 2-positive is shown; positivity (dashed line) defined as 2 s.d. above the mean score of the unvaccinated (Naive) NHPs. **h**, Volcano plot showing differentially expressed genes between T cells positive and negative for module 2 at week 13 (P values calculated using the likelihood ratio test with Bonferroni correction).

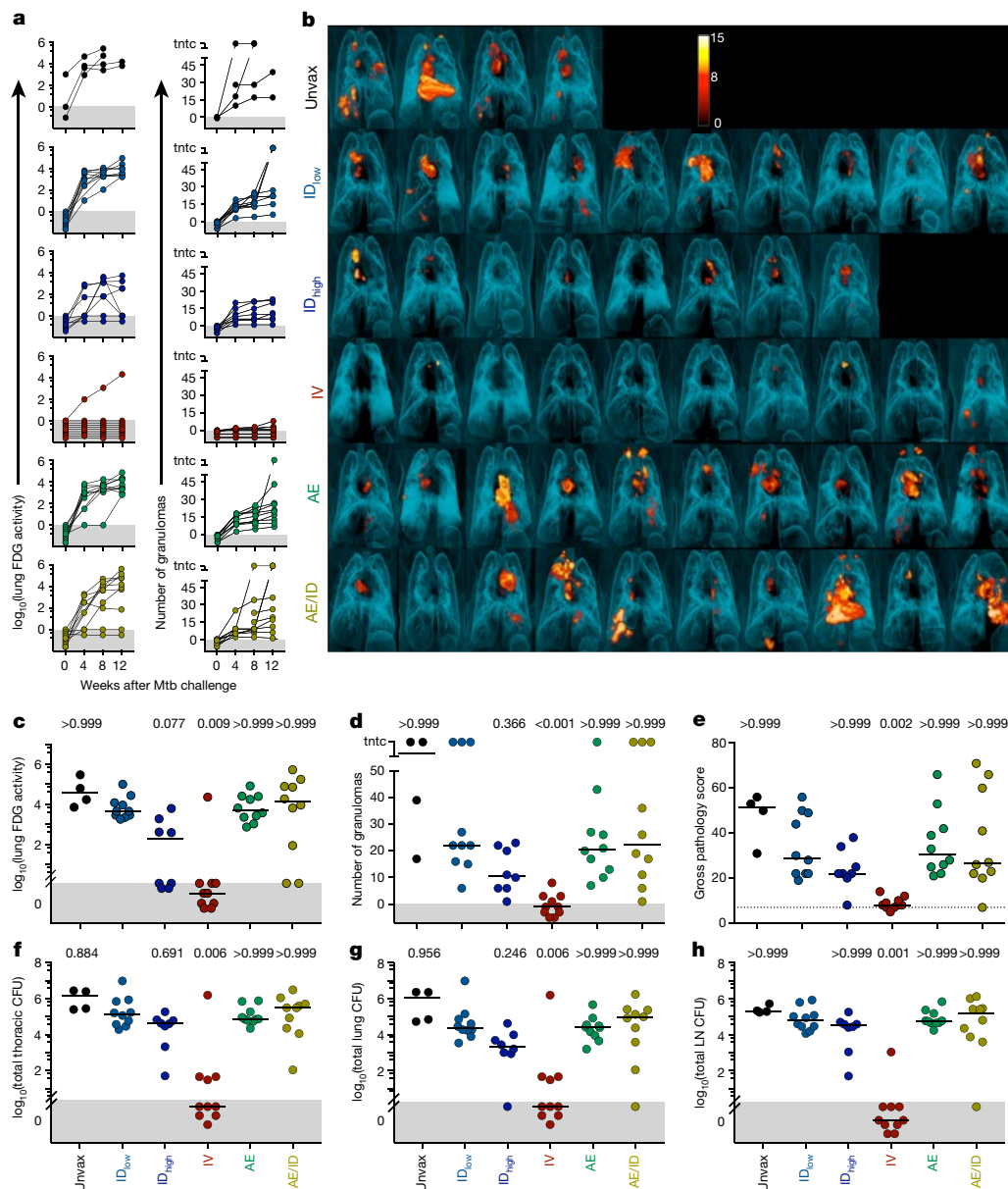


Fig. 2 | Protection against Mtb infection after IV BCG immunization. **a**, Lung inflammation (total FDG activity) and number of lung granulomas over the course of infection as measured by serial PET–CT scans. Each line shows one NHP over time; 3 NHPs (2 unvaccinated (unvax) and 1 ID_{low}) reached a humane end point before 12 weeks. tntc, too numerous to count. **b**, Three-dimensional volume renderings of PET–CT scans of each NHP at the time of necropsy. PET was limited to the thoracic cavity; the standardized uptake value colour bar is shown in the top right and indicates FDG retention, a surrogate for inflammation. **c–h**, Total lung FDG activity (**c**), number of lung granulomas (**d**),

gross pathology score (**e**), total thoracic CFUs (mycobacterial burden) (**f**), total lung CFUs (**g**) and total thoracic LN CFUs (**h**) at time of necropsy. Dashed line in **e** is assumed normal pathology score accounting for variability in LN size in healthy rhesus macaques. **c–h**, Symbols represent individual challenged macaques (cohorts 1–3, $n = 8–10$ vaccinated NHPs; $n = 4$ unvaccinated NHPs) and horizontal bars represent the median; all data points within the grey areas are zero. Kruskal–Wallis tests were used and reported P values represent Dunn’s multiple comparison test comparing each group to the ID_{low} group.

showed that the IV-BCG-immunized group had lower gross pathology scores²⁷ (Fig. 2e) compared with the ID_{low} BCG group ($P = 0.002$) and was the only group without detectable extrapulmonary disease (Extended Data Fig. 8a).

The primary measure of protection was a comprehensive quantification of Mtb burden (CFUs) at necropsy. The median total thoracic CFUs for ID_{low} BCG (5.1 ± 1.3 , median \pm interquartile range of \log_{10} -transformed total CFUs) was slightly lower than that of unvaccinated NHPs (5.9 ± 1.0 \log_{10} -transformed CFUs), consistent with ID_{low} BCG having a minimal protective effect in rhesus macaques (Fig. 2f). By contrast, the median total thoracic CFUs in IV-BCG-immunized NHPs was $0 (\pm 16)$ CFUs—a more than 100,000-fold reduction compared with

ID_{low} BCG ($P = 0.006$). Six out of ten IV-BCG-immunized macaques had no detectable Mtb in any tissue measured, and another three macaques had ≤ 45 total CFUs, all contained within one granuloma. Only one of ten IV BCG NHPs was not protected, with CFU values similar to ID_{low} NHPs (Fig. 2f). The ID_{high} , AE and AE/ID groups had bacterial burdens similar to ID_{low} BCG.

Total thoracic bacterial burden can be separated into lung (Fig. 2g) and thoracic lymph node (LN) (Fig. 2h) CFUs. Only the IV BCG group was lower than the ID_{low} BCG group (lung, $P = 0.006$; LNs, $P = 0.001$), with nine of ten NHPs having no Mtb-positive LNs (Fig. 2h).

Protection can be defined as having less than a given number of total thoracic Mtb CFUs. By this criterion, protection was highly significant

(Fisher's exact test, $P < 10^{-4}$) at any given threshold less than 10,000 CFUs (Extended Data Fig. 8b), with the IV BCG group showing 90% protection (95% confidence interval: 60–98%) at a threshold as low as 50 CFUs. Thus, BCG IV confers an unprecedented degree of protection in a stringent NHP model of TB.

Immune responses after Mtb challenge

Measuring immune responses after challenge informs whether vaccine-elicited responses are boosted (anamnestic), and if de novo (primary) responses are generated to antigens expressed by the challenge microorganism (but not the vaccine). T cell responses to ESAT-6 and CFP-10—proteins expressed in Mtb but not BCG—are used to detect primary Mtb infection, even in BCG-immunized individuals. Peripheral T cell and antibody responses to these Mtb-specific antigens and those expressed by both BCG and Mtb (for example, PPD), were assessed after Mtb challenge (Extended Data Fig. 9). In contrast to all other groups, IV-BCG-immunized NHPs had low to undetectable primary or anamnestic T cell and antibody responses after TB infection, which suggests rapid elimination of Mtb after challenge.

BCG and immune responses in tissues

To provide insight into the potential mechanisms of IV-BCG-induced protection, we quantified BCG CFUs and T cell responses in tissues 1 month after vaccination. BCG was detected at the skin site(s) of injection and draining axillary LNs in ID-BCG-vaccinated NHPs, but not in lung lobes (Fig. 3a). In AE- or AE/ID-BCG-vaccinated NHPs, BCG was detected primarily in lung lobes and BAL. By contrast, BCG was detected in the spleen of all four IV-BCG-vaccinated NHPs, as well as in BAL, lung lobe, and peripheral and lung LNs (Fig. 3a). Indeed, PET–CT scans at 2 and 4 weeks after BCG vaccination showed increased metabolism localized to lung LNs, lung lobes and spleen elicited by the IV but not by other routes (Extended Data Fig. 10a).

CD4 T cell responses in IV-BCG-immunized NHPs were increased in spleen and lung compared to ID_{low} NHPs (Fig. 3b), consistent with detection of BCG at the same sites. Moreover, CD4 T cell responses were observed in systemic sites such as PBMCs, bone marrow and peripheral LNs. CD8 responses were highest in lung lobes, BAL and spleen after IV BCG (Fig. 3c). After ID_{high} BCG vaccination, CD4 T cell responses were detected in spleen, bone marrow and axillary LNs, but were limited in lung lobes and lung LNs, whereas responses in AE groups were confined to the lung and BAL. Collectively, these data indicate compartmentalization of BCG detection and T cell immunity by vaccine route, which highlights the systemic distribution of immune responses after IV BCG versus the more limited and localized responses following ID and AE delivery.

Further analysis of lung tissue one month after vaccination showed increased cell counts (Fig. 3d) after IV BCG with increased numbers of CD3⁺ T cells and CD11c⁺ antigen-presenting cells (Fig. 3e). These clustered into 'microgranulomas' that were histologically distinct from bronchus-associated lymphoid tissue (BALT) (Fig. 3f). IV-BCG-vaccinated macaques had transient splenomegaly as well as enlarged thoracic LNs that contained non-necrotizing granulomas and lymphoid follicular hyperplasia, often with active germinal centres (Extended Data Fig. 10b–e).

Six months after BCG vaccination (time of challenge), NHPs that received IV BCG maintained increased frequencies of antigen-responsive T cells in spleen, lung and BAL (Extended Data Fig. 11a, b). Notably, the numbers of total, CD3⁺ or CD11c⁺ cells in lung tissue had normalized, and lung histopathology, spleen size and FDG uptake in IV-BCG-vaccinated macaques were indistinguishable from ID_{low} BCG macaques (Extended Data Fig. 11c–g). Although BCG burden was not measured in these NHPs, no BCG (or Mtb) CFUs were detected in six out of ten IV-BCG-immunized, challenged macaques at 9 months after BCG.

Collectively, these data suggest that BCG is cleared between 1 and 9 months after IV vaccination.

T cells in lung tissue after BCG

To substantiate whether T cells isolated from lung lobes one month after IV BCG were T_{RM} cells, labelled anti-CD45 antibody was injected IV into NHPs just before necropsy—a technique shown to delineate tissue-derived (ivCD45⁺) from vasculature-derived (ivCD45⁺) leukocytes^{29,30}. Ex vivo phenotypic analysis of CD69 expression (a marker of T_{RM} and/or T cell activation) in combination with ivCD45 staining revealed that more than 80% of CD4 T cells isolated from all lung lobes of IV-BCG-immunized NHPs were derived from the lung parenchyma (CD69⁺ivCD45⁺) (Fig. 4a). Of note, more than 1,000 BCG CFUs were cultured from every lung lobe in this macaque. By contrast, ID_{high} and AE BCG vaccination resulted in 16–35% tissue-derived (CD69⁺ivCD45⁺) CD4 T cells in the lung lobes, with few or undetectable BCG CFUs. T cells from BAL in all NHPs were uniformly CD69⁺ivCD45⁺. Similar results were observed in the CD8 T cell compartment of the same macaques (Supplementary Data 7).

After in vitro antigen stimulation to assess antigen-responsive T cells in tissue, lung tissue-derived (ivCD45⁺) IFN γ -producing CD4 T cells were observed in all lung lobes and lung LNs of IV-BCG-immunized NHPs (Fig. 4b and Extended Data Fig. 12). Antigen-responsive lung T cells were largely CD69⁺ with a subset also expressing the tissue-homing marker CD103, which is expressed on some T_{RM} cells³¹ (Fig. 4c). Thus, these cells may represent bona fide T_{RM} cells, or recently activated T cells owing to the presence of BCG (Fig. 4a). Overall, these data show that IV BCG vaccination provided the highest level of protection concomitant with increased antigen-responsive T cells throughout lung tissue.

The increased detection of T cell responses in tissues containing BCG suggests that alternative approaches to lung vaccine delivery may be crucial for generating T_{RM} cells. Indeed, direct endobronchial instillation of BCG into a single lung lobe protected two out of eight NHPs against Mtb challenge in the same lobe³². To determine how endobronchial BCG would affect T cells in the lung parenchyma, BCG was instilled directly into the left lung lobes of NHPs. Approximately 75% of CD4 and CD8 T cells isolated from the two left lung lobes were CD69⁺ivCD45⁺, compared with 7–45% in the right lobes (Fig. 4a and Supplementary Data 7a). Notably, BCG CFUs (>10⁴) were detected in the left (but not right) lung lobes where the CD4 T cell response was highest (Extended Data Fig. 12). Collectively, these data suggest a general concordance between the presence of BCG in a given tissue after vaccination and the detection of antigen-responsive T cells.

Immune associations of bacterial control

Several multiple regressions were used to test whether peak antigen-responsive CD4 or CD8 T cells in the BAL or PBMCs after BCG immunization were associated with disease severity (Extended Data Fig. 13, Supplementary Tables 1 and 5). These analyses show that the route of BCG vaccination was the primary determinant of Mtb control with IV being the only regimen that afforded significant protection (Extended Data Fig. 8b).

Discussion

The data demonstrating that IV BCG immunization results in markedly increased antigen-responsive T cells, including T cells systemically and throughout the lung parenchyma, and unprecedented protection against Mtb challenge, represent a major step forward in the field of TB vaccine research.

The concept of alternative immunization routes rather than the standard ID approach was suggested 50 years ago in NHP studies comparing IV and AE immunization^{5–8}. More recently, decreased lung pathology

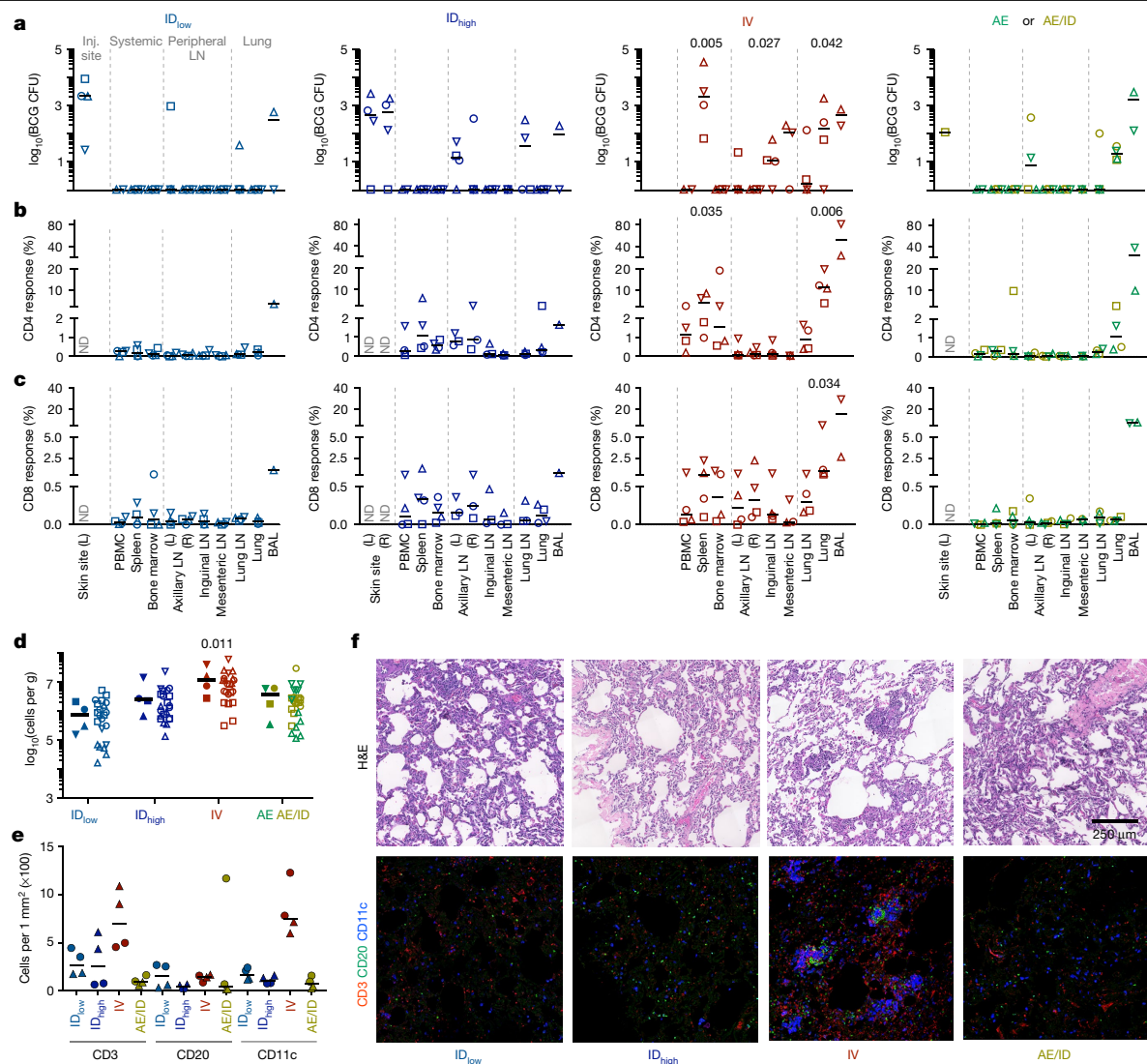


Fig. 3 | BCG CFUs and immune responses in tissues one month after BCG immunization. NHPs (cohorts 5a–c: ID_{low}, ID_{high} and IV, $n = 4$ NHPs; AE and AE/ID, $n = 2$ NHPs) were euthanized one month after vaccination to quantify BCG and T cell responses in tissues. **a**, BCG CFUs at vaccination site(s) (skin, ID only) and in various tissues (per ml blood or bone marrow; per whole spleen, LN or lung lobe; or per total BAL collected). L, left; R, right; ND, not determined. **b, c**, Frequency of memory CD4 (**b**) and CD8 (**c**) T cells producing IFN γ , IL-2, TNF or IL-17 after PPD stimulation. Matched symbols within each vaccine group are the same macaque. Kruskal–Wallis tests were run and reported P values represent Dunn’s multiple comparison test comparing each group to the ID_{low} group. **d**, Total viable cells per gram of lung tissue for each vaccine regimen;

data are shown as the median of four macaques per group (solid symbols, six lung lobes from each NHP are averaged) or as counts for each lung lobe ($n = 24$ lobes) from all NHPs (open symbols with lobes from same macaque matched). Kruskal–Wallis test was run on medians; Dunn’s adjusted P values are from comparing each group to the ID_{low} group. **e**, Quantification of CD3⁺, CD20⁺ and CD11c⁺ cells from two lung sections per NHP (matched symbols, $n = 2$ macaques). **f**, Representative (one out of four) 1 mm² lung sections from each BCG regimen stained with haematoxylin and eosin (H&E; top) or with antibodies against CD3⁺ T cells (red), CD20⁺ B cells (green), and CD11c⁺ macrophages or dendritic cells (blue).

and a trend towards increased survival was reported after IV BCG immunization compared with unvaccinated NHPs³³. AE immunization with an attenuated Mtb strain enhanced cellular immunity in the BAL, and reduced lung pathology and bacterial burdens, after high-dose challenge 8 weeks later with a low virulence Mtb strain (CDC1551)³⁴. In different method of pulmonary delivery, BCG instilled directly into the lower left lung lobe (that is, endobronchially), prevented infection and disease in two out of eight NHPs after repeated limiting-dose Mtb challenge in the same lung lobe, starting 13 weeks after vaccination³². The robust and localized T cell responses in lung tissue after direct BCG instillation (Fig. 4a and Extended Data Fig. 12d) provide a potential mechanistic difference between direct endobronchial and AE delivery that could influence protection. Finally, a cytomegalovirus (CMV) vector encoding

Mtb antigens prevented TB disease in 14 out of 34 macaques across two studies, with 10 out of 14 being Mtb culture-negative³⁵. In contrast to IV BCG immunization, all CMV-immunized macaques generated primary responses to Mtb antigens after challenge, suggesting that these vaccines elicit distinct mechanisms or kinetics of protection.

There are at least three immune mechanisms for how IV BCG may mediate protection. First, rapid elimination of Mtb may be due to the high magnitude of T cell responses in lung tissue. Our data are consistent with studies in mice that demonstrate the superior capacity of lung-localized T_{RM} cells to control TB disease^{36,37}, and studies in NHPs showing that depletion of lung interstitial CD4 T cells during SIV infection of Mtb latently infected NHPs is associated with reactivation and dissemination³⁸. Second, there is some evidence that antibodies can

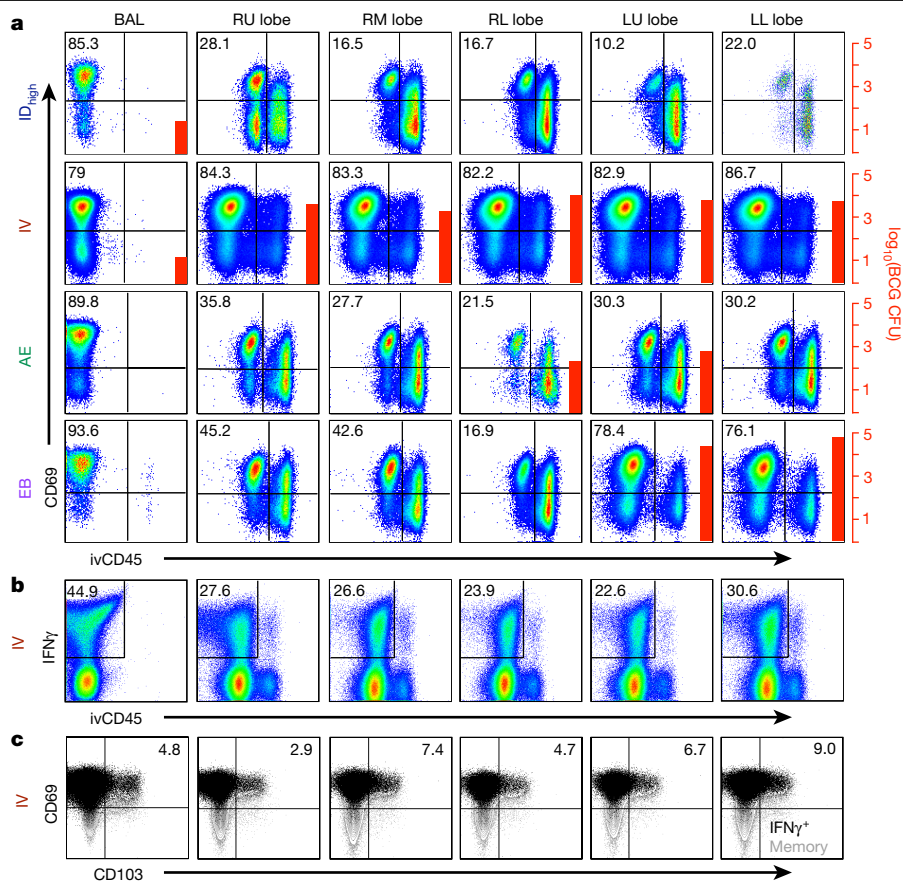


Fig. 4 | Detection of T cells in lung tissue after IV BCG immunization. a, One month after BCG vaccination, tissue-derived versus blood-derived cells in lung were delineated by injecting NHPs with a fluorochrome-conjugated anti-CD45 antibody (ivCD45) to label leukocytes in the vasculature. NHPs (cohort 6, $n = 2$ macaques) received 5×10^7 CFUs BCG ID, IV, AE or endobronchially (EB) into the left lung. At necropsy, BCG CFUs were quantified in tissues and cells were stained immediately ex vivo for surface marker expression (**a**) or stimulated with *Mtb* whole-cell lysate (WCL) and stained for cytokine production (**b**, **c**).

Plots show CD4 T cells from the BAL and lung lobes (RU, right upper; RM, right middle; RL, right lower; LU, left upper; LL, left lower) from one of two macaques per BCG regimen. **a**, Percentage of ivCD45⁻ (unstimulated) CD4 T cells expressing the tissue-resident/activation marker CD69; BCG CFUs (if detected) are indicated by red bars and right scale. **b**, Percentage of WCL-responsive (IFN γ ⁺) CD4 T cells in BAL and lung tissue (ivCD45⁻) and (**c**) the percentage of IFN γ ⁺ CD4 memory T cells expressing CD69 and CD103 after IV BCG vaccination.

mediate control against *Mtb* in vivo or in vitro^{39,40}. Antibody levels were higher in the BAL and plasma after IV BCG compared with other routes of vaccination, but declined to pre-vaccination levels in the BAL at the time of challenge (Extended Data Fig. 7). Third, IV BCG vaccination in mice induced epigenetically modified macrophages with enhanced capacity to protect against *Mtb* infection⁴¹, a process termed ‘trained immunity’^{14,15}. Such an effect was dependent on BCG being detectable in the bone marrow; this was not observed one month after IV BCG vaccination in NHPs (Fig. 3a). Moreover, there was no increase in innate activation of PBMCs to non-*Mtb* antigens after IV BCG vaccination—a hallmark of trained immunity (Supplementary Data 3). Nonetheless, it is possible that any of these three mechanisms might act independently or together to mediate protection.

Because nine out of ten macaques were protected by IV BCG immunization (Fig. 2), we were unable to define an immune correlate of protection within this group (Extended Data Fig. 13); however, there were several unique quantitative and qualitative differences in the immune responses after IV BCG vaccination that may underlie protection. First, there were substantially higher numbers of *Mtb* antigen-responsive T cells in the BAL and PBMCs (Fig. 1b–e). Second, there was a unique CD4 T cell transcriptional profile in the BAL, which included upregulation of genes that have been associated with protection against TB (Fig. 1f–h). Third, and perhaps most noteworthy, was the large population of T cells in the tissue across all lung parenchyma lobes (Fig. 4, Extended Data

Fig. 12 and Supplementary Data 7). Notably, although the BAL CD4 T cell responses were higher in ID_{high}⁻, AE- and AE/ID-BCG-immunized NHPs compared to the ID_{low} BCG group, there was no increased protection. These data suggest that although measurement of BAL responses may provide greater insight into vaccine efficacy compared to blood, they may not fully reflect lung T_{RM} cell responses that might be the mechanism of protection.

In conclusion, this study provides a paradigm shift towards developing vaccines focused on preventing TB infection to prevent latency, active disease and transmission. The data support clinical development of IV delivery of BCG for use in adolescents or adults in whom modelling predicts the greatest effect on TB transmission³, and suggest that the IV route may improve the protective capacity of other vaccine platforms. This study also provides a benchmark against which future vaccines will be tested and a new framework to understand the immune correlates and mechanisms of protection against TB.

Online content

Any methods, additional references, Nature Research reporting summaries, source data, extended data, supplementary information, acknowledgements, peer review information; details of author contributions and competing interests; and statements of data and code availability are available at <https://doi.org/10.1038/s41586-019-1817-8>.

1. World Health Organization. *Global Tuberculosis Report* https://www.who.int/tb/publications/global_report/en/ (2018).
2. Mangtani, P. et al. Protection by BCG vaccine against tuberculosis: a systematic review of randomized controlled trials. *Nephrol. Dial. Transplant.* **58**, 470–480 (2014).
3. Harris, R. C., Sumner, T., Knight, G. M. & White, R. G. Systematic review of mathematical models exploring the epidemiological impact of future TB vaccines. *Hum. Vaccin. Immunother.* **12**, 2813–2832 (2016).
4. Cooper, A. M. Cell-mediated immune responses in tuberculosis. *Annu. Rev. Immunol.* **27**, 393–422 (2009).
5. Barclay, W. R., Anacker, R. L., Brehmer, W., Leif, W. & Ribi, E. Aerosol-induced tuberculosis in subhuman primates and the course of the disease after intravenous BCG vaccination. *Infect. Immun.* **2**, 574–582 (1970).
6. Ribi, E. et al. Efficacy of mycobacterial cell walls as a vaccine against airborne tuberculosis in the rhesus monkey. *J. Infect. Dis.* **123**, 527–538 (1971).
7. Anacker, R. L. et al. Superiority of intravenously administered BCG and BCG cell walls in protecting rhesus monkeys (*Macaca mulatta*) against airborne tuberculosis. *Z. Immunitätsforsch. Exp. Klin. Immunol.* **143**, 363–376 (1972).
8. Barclay, W. R. et al. Protection of monkeys against airborne tuberculosis by aerosol vaccination with bacillus Calmette–Guerin. *Am. Rev. Respir. Dis.* **107**, 351–358 (1973).
9. Greene, J. M. et al. MR1-restricted mucosal-associated invariant T (MAIT) cells respond to mycobacterial vaccination and infection in nonhuman primates. *Mucosal Immunol.* **10**, 802–813 (2017).
10. Joosten, S. A. et al. Harnessing donor unrestricted T-cells for new vaccines against tuberculosis. *Vaccine* **37**, 3022–3030 (2019).
11. Qaqish, A. et al. Adoptive transfer of phosphoantigen-specific $\gamma\delta$ T cell subset attenuates *Mycobacterium tuberculosis* infection in nonhuman primates. *J. Immunol.* **198**, 4753–4763 (2017).
12. Roy Chowdhury, R. et al. A multi-cohort study of the immune factors associated with *M. tuberculosis* infection outcomes. *Nature* **560**, 644–648 (2018).
13. Suliman, S. et al. Bacillus Calmette–Guerin (BCG) revaccination of adults with latent *Mycobacterium tuberculosis* infection induces long-lived BCG-reactive NK cell responses. *J. Immunol.* **197**, 1100–1110 (2016).
14. Joosten, S. A. et al. Mycobacterial growth inhibition is associated with trained innate immunity. *J. Clin. Invest.* **128**, 1837–1851 (2018).
15. Kleinnijenhuis, J. et al. Long-lasting effects of BCG vaccination on both heterologous Th1/Th17 responses and innate trained immunity. *J. Innate Immun.* **6**, 152–158 (2014).
16. Khader, S. A. et al. IL-23 and IL-17 in the establishment of protective pulmonary CD4⁺ T cell responses after vaccination and during *Mycobacterium tuberculosis* challenge. *Nat. Immunol.* **8**, 369–377 (2007).
17. Gideon, H. P. et al. Variability in tuberculosis granuloma T cell responses exists, but a balance of pro- and anti-inflammatory cytokines is associated with sterilization. *PLoS Pathog.* **11**, e1004603 (2015).
18. Soares, A. P. et al. Longitudinal changes in CD4⁺ T-cell memory responses induced by BCG vaccination of newborns. *J. Infect. Dis.* **207**, 1084–1094 (2013).
19. Darrah, P. A. et al. Multifunctional T_H1 cells define a correlate of vaccine-mediated protection against *Leishmania major*. *Nat. Med.* **13**, 843–850 (2007).
20. Lewinsohn, D. A., Lewinsohn, D. M. & Scriba, T. J. Polyfunctional CD4⁺ T cells as targets for tuberculosis vaccination. *Front. Immunol.* **8**, 1262 (2017).
21. Chattopadhyay, P. K., Yu, J. & Roederer, M. Live-cell assay to detect antigen-specific CD4⁺ T-cell responses by CD154 expression. *Nat. Protocols* **1**, 1–6 (2006).
22. Orr, M. T. et al. Interferon γ and tumor necrosis factor are not essential parameters of CD4⁺ T-cell responses for vaccine control of tuberculosis. *J. Infect. Dis.* **212**, 495–504 (2015).
23. Sakai, S. et al. CD4 T cell-derived IFN- γ plays a minimal role in control of pulmonary *Mycobacterium tuberculosis* infection and must be actively repressed by PD-1 to prevent lethal disease. *PLoS Pathog.* **12**, e1005667 (2016).
24. Gierahn, T. M. et al. Seq-Well: portable, low-cost RNA sequencing of single cells at high throughput. *Nat. Methods* **14**, 395–398 (2017).
25. Sallin, M. A. et al. Host resistance to pulmonary *Mycobacterium tuberculosis* infection requires CD153 expression. *Nat. Microbiol.* **3**, 1198–1205 (2018).
26. Booty, M. G. et al. IL-21 signaling is essential for optimal host resistance against *Mycobacterium tuberculosis* infection. *Sci. Rep.* **6**, 36720 (2016).
27. Maiello, P. et al. Rhesus macaques are more susceptible to progressive tuberculosis than cynomolgus macaques: a quantitative comparison. *Infect. Immun.* **86**, e00505-17 (2018).
28. Darrah, P. A. et al. Boosting BCG with proteins or rAd5 does not enhance protection against tuberculosis in rhesus macaques. *Vaccines (Basel)* **4**, 21 (2019).
29. Anderson, K. G. et al. Intravascular staining for discrimination of vascular and tissue leukocytes. *Nat. Protocols* **9**, 209–222 (2014).
30. Kauffman, K. D. et al. Defective positioning in granulomas but not lung-homing limits CD4 T-cell interactions with *Mycobacterium tuberculosis*-infected macrophages in rhesus macaques. *Mucosal Immunol.* **11**, 462–473 (2018).
31. Masopust, D. & Soerens, A. G. Tissue-resident T cells and other resident leukocytes. *Annu. Rev. Immunol.* **37**, 521–546 (2019).
32. Dijkman, P. A. et al. Prevention of tuberculosis infection and disease by local BCG in repeatedly exposed rhesus macaques. *Nat. Med.* **25**, 255–262 (2019).
33. Sharpe, S. et al. Alternative BCG delivery strategies improve protection against *Mycobacterium tuberculosis* in non-human primates: protection associated with mycobacterial antigen-specific CD4 effector memory T-cell populations. *Tuberculosis (Edinb.)* **101**, 174–190 (2016).
34. Kaushal, D. et al. Mucosal vaccination with attenuated *Mycobacterium tuberculosis* induces strong central memory responses and protects against tuberculosis. *Nat. Commun.* **6**, 8533 (2015).
35. Hansen, S. G. et al. Prevention of tuberculosis in rhesus macaques by a cytomegalovirus-based vaccine. *Nat. Med.* **24**, 130–143 (2018).
36. Moguche, A. O. et al. ICOS and Bcl6-dependent pathways maintain a CD4 T cell population with memory-like properties during tuberculosis. *J. Exp. Med.* **212**, 715–728 (2015).
37. Sakai, S. et al. Cutting edge: control of *Mycobacterium tuberculosis* infection by a subset of lung parenchyma-homing CD4 T cells. *J. Immunol.* **192**, 2965–2969 (2014).
38. Corleis, B. et al. HIV-1 and SIV infection are associated with early loss of lung interstitial CD4⁺ T cells and dissemination of pulmonary tuberculosis. *Cell Reports* **26**, 1409–1418 (2019).
39. Lu, L. L. et al. A functional role for antibodies in tuberculosis. *Cell* **167**, 433–443 (2016).
40. Li, H. & Javid, B. Antibodies and tuberculosis: finally coming of age? *Nat. Rev. Immunol.* **18**, 591–596 (2018).
41. Kaufmann, E. et al. BCG educates hematopoietic stem cells to generate protective innate immunity against tuberculosis. *Cell* **172**, 176–190 (2018).

Publisher's note Springer Nature remains neutral with regard to jurisdictional claims in published maps and institutional affiliations.



Open Access This article is licensed under a Creative Commons Attribution 4.0 International License, which permits use, sharing, adaptation, distribution and reproduction in any medium or format, as long as you give appropriate credit to the original author(s) and the source, provide a link to the Creative Commons license, and indicate if changes were made. The images or other third party material in this article are included in the article's Creative Commons license, unless indicated otherwise in a credit line to the material. If material is not included in the article's Creative Commons license and your intended use is not permitted by statutory regulation or exceeds the permitted use, you will need to obtain permission directly from the copyright holder. To view a copy of this license, visit <http://creativecommons.org/licenses/by/4.0/>.

© The Author(s) 2019

Methods

Macaques and sample size

Indian-origin rhesus macaques (*Macaca mulatta*) used in these studies are outlined in Extended Data Fig. 1c and Supplementary Table 1. All experimentation complied with ethical regulations at the respective institutions (Animal Care and Use Committees of the Vaccine Research Center, NIAID, NIH and of Bioqual, Inc., and of the Institutional Animal Care and Use Committee of the University of Pittsburgh). Macaques were housed and cared for in accordance with local, state, federal, and institute policies in facilities accredited by the American Association for Accreditation of Laboratory Animal Care (AAALAC), under standards established in the Animal Welfare Act and the Guide for the Care and Use of Laboratory Animals. Macaques were monitored for physical health, food consumption, body weight, temperature, complete blood counts, and serum chemistries. All infections were performed at the University of Pittsburgh where animals were housed in a biosafety level 3 facility.

The sample size for this study was determined using bacterial burden (measured as \log_{10} -transformed total thoracic CFUs) as the primary outcome variable. Initially, we planned to test BCG route efficacy by comparing IV, AE and AE/ID routes to ID_{low} vaccination and found that ten macaques per group would be sufficient to obtain over 90% power and adjusted the type I error rate for three group comparisons ($\alpha = 0.0167$). After initiation of the first cohort of NHPs in this study, we elected to test the effect of dose on ID vaccination by adding an ID_{high} group ($n = 8$ macaques). The additional treatment group did not substantially reduce the power of the study. To detect a 1.5 difference in \log_{10} (total CFUs) with a pooled standard deviation of 0.8 (using previous data), we obtained over 90% (90.7%) power using 10 macaques per group with an adjusted type I error rate for 4 group comparisons ($\alpha = 0.0125$). The comparison made between the ID_{high} ($n = 8$ macaques) and ID_{low} ($n = 10$ macaques) groups achieved 85.6% power detecting the same difference ($\log_{10}(1.5)$) and with an $\alpha = 0.0125$.

BCG vaccination

For Mtb challenge studies (cohorts 1–3), 3–5-year-old male ($n = 32$) and female ($n = 20$) rhesus macaques were randomized into experimental groups based on gender, weight and pre-vaccination CD4 T cell responses to PPD in BAL. Macaques were vaccinated at Bioqual, Inc. under sedation and in successive cohorts as outlined in Extended Data Fig. 1c. BCG Danish Strain 1331 (Statens Serum Institute, Copenhagen, Denmark) was expanded⁴², frozen at approximately 3×10^8 CFUs ml⁻¹ in single-use aliquots and stored at -80°C . Immediately before injection, BCG (for all vaccine routes) was thawed and diluted in cold PBS containing 0.05% tyloxapol (Sigma-Aldrich) and 0.002% antifoam Y-30 (Sigma-Aldrich) to prevent clumping of BCG and foaming during aerosolization⁴³. For ID vaccinations, BCG was injected in the left upper arm (5×10^5 CFUs; ID_{low}) or split across both upper arms (5×10^7 CFUs; ID_{high}) in a volume of 100–200 μl per site. IV BCG (5×10^7 CFUs) was injected into the left saphenous vein in a volume of 2 ml; AE BCG (5×10^7 CFUs) was delivered in a 2 ml volume via paediatric mask attached to a Pari eFlow nebulizer (PARI Pharma GmbH) that delivered 4 μM particles into the lung, as previously described²⁸; AE/ID macaques were immunized simultaneously (5×10^7 CFUs AE plus 5×10^5 CFUs ID in left arm); EB BCG (5×10^7 CFUs in 2 ml; cohort 6 only) was instilled into the left lung lobes using an endoscope. No loss of viability was observed for BCG after aerosolization. In pilot studies, lower doses of BCG were prepared and delivered as described above. Text refers to nominal BCG doses—actual BCG CFUs for vaccine regimens in every cohort were quantified immediately after vaccination and are reported in Extended Data Fig. 1c and Supplementary Table 1.

Mtb challenge

Macaques (cohorts 1–3) were challenged by bronchoscope with 4–36 CFUs barcoded Mtb Erdman 6–10 months after BCG vaccination (Extended Data Fig. 1c and Supplementary Table 1) in a 2 ml volume

as previously described⁴⁴. Infectious doses across this range result in similar levels of TB disease in unvaccinated rhesus in this and previous studies²⁸ (Supplementary Data 12). Clinical monitoring included regular monitoring of appetite, behaviour and activity, weight, erythrocyte sedimentation rate, Mtb growth from gastric aspirate and coughing. These signs, as well as PET–CT characteristics, were used as criteria in determining whether a macaque met the humane end point before the pre-determined study end point.

PET–CT scans and analysis

PET–CT scans were performed using a microPET Focus 220 preclinical PET scanner (Siemens Molecular Solutions) and a clinical eight-slice helical CT scanner (NeuroLogica Corporation) as previously described^{27,45–47}. 2-deoxy-2-(¹⁸F)fluorodeoxyglucose (FDG) was used as the PET probe. Serial scans were performed before, 4 and 8 weeks after Mtb, and before necropsy (cohorts 1–3) or at 2 and 4 weeks after BCG (cohorts 5a, b). OsiriX MD (v.10.0.1), a DICOM (Digital Imaging and Communications in Medicine) image viewer, was used for scan analyses, as described⁴⁷. Lung inflammation was measured as total FDG activity within the lungs. A region of interest (ROI) was segmented which encompassed all lung tissue on CT and was then transferred to the co-registered PET scan. On the PET scan, all image voxels of FDG-avid pathology (Standard Uptake Value >2.3) were isolated and summated resulting in a cumulative standardized uptake value. To account for basal metabolic FDG uptake, total FDG activity was normalized to resting muscle resulting in a total lung inflammation value. Individual granulomas were counted on each CT scan. If granulomas were too small and numerous within a specific area to count individually or if they consolidated, quantification was considered to be too numerous to count. To measure the volume of the spleen, an ROI was drawn outlining the entire organ on each of the axial slices of the CT scan and the volume was computed across these ROIs (using a tool in OsiriX). Any scans for which visibility of the entire spleen was limited ($n = 2$ macaques) were excluded from this analysis.

Necropsy, pathology scoring and Mtb and BCG burden

For challenge studies (cohorts 1–3), NHPs were euthanized 11–15 weeks after Mtb or at humane endpoint by sodium pentobarbital injection, followed by gross examination for pathology. A published scoring system²⁷ was used to determine total pathology from each lung lobe (number and size of lesions), LN (size and extent of necrosis), and extrapulmonary compartments (number and size of lesions). All granulomas and other lung pathologies, all thoracic LNs, and peripheral LNs were matched to the final PET–CT scan and collected for quantification of Mtb. Each lesion (including granulomas, consolidations and clusters of granulomas) in the lung, all thoracic LNs, random sampling (50%) of each of the 7 lung lobes, 3–5 granulomas (if present) or random samples (30%) of spleen and liver, and any additional pathologies were processed to comprehensively quantify bacterial burdens. Suspensions were plated on 7H11 agar (Difco) and incubated at 37°C with 5% CO_2 for 3 weeks for CFU enumeration or formalin-fixed and paraffin-embedded for histological examination. CFUs were counted and summed to calculate the total thoracic bacterial burden for the macaque^{17,27,48}. Mtb CFUs for every challenged macaque are listed in Supplementary Table 1.

To determine BCG CFUs, BAL, bone marrow aspirates, and blood were collected from NHPs before euthanasia. Individual lung lobes and thoracic and peripheral LNs, spleen, liver, and the skin site(s) of injection (if applicable) were excised. 0.5 ml of blood and bone marrow and 10% of retrieved BAL wash fluid were plated; approximately 1 g of tissue (or one whole LN or skin biopsy) was processed in water in gentleMACS M Tubes (Miltenyi Biotec) using a gentleMACS Dissociator (Miltenyi Biotec). Samples were plated and counted as above. Data are reported as CFUs ml⁻¹ of blood or bone marrow, CFUs per total BAL collected, CFUs per one LN or skin biopsy, CFUs per lung lobe or spleen. CFUs from individual lung lobes and LNs of the same category (for example, hilar) were averaged for each NHP.

Rhesus blood, BAL and tissue processing

Blood PBMCs were isolated using Ficoll-Paque PLUS gradient separation (GE Healthcare Biosciences) and standard procedures; BAL wash fluid (3×20 ml washes of PBS) was centrifuged and cells were combined before counting, as described²⁸. LNs were mechanically disrupted and filtered through a 70- μ m cell strainer. Lung and spleen tissues were processed using gentleMACS C Tubes and Dissociator in RPMI 1640 (ThermoFisher Scientific). Spleen mononuclear cells were further separated using Ficoll-Paque. Lung tissue was digested using collagenase, Type I (ThermoFisher Scientific) and DNase (Sigma-Aldrich) for 30–45 min at 37 °C with shaking, followed by passing through a cell strainer. Single-cell suspensions were resuspended in warm R10 (RPMI 1640 with 2 mM L-glutamine, 100 U ml⁻¹ penicillin, 100 μ g ml⁻¹ streptomycin, and 10% heat-inactivated FBS; Atlantic Biologicals) or cryopreserved in FBS containing 10% DMSO in liquid nitrogen.

Multiparameter flow cytometry

Generally, longitudinal PBMC samples were batch-analysed for antigen-specific T cell responses or cellular composition at the end of the study from cryopreserved samples whereas BAL and tissue (necropsy) samples were analysed fresh. Cryopreserved PBMC were washed, thawed and rested overnight in R10 before stimulation, as described²⁸. For T cell stimulation assays, 1–5 million viable cells were plated in 96-well V-bottom plates (Corning) in R10 and incubated with R10 alone (background), or with 20 μ g ml⁻¹ tuberculin PPD (Statens Serum Institut, Copenhagen, Denmark), 20 μ g ml⁻¹ H37Rv Mtb WCL (BEI Resources), or 1 μ g ml⁻¹ each of ESAT-6 and CFP-10 peptide pools (provided by Aeras, Rockville, MD) for 2 h before adding 10 μ g ml⁻¹ BD GolgiPlug (BD Biosciences). The concentrations of PPD and WCL were optimized to detect CD4 T cell responses; however, protein antigen stimulation may underestimate CD8 T cell responses. For logistical reasons, cells were stimulated overnight (14 h total) before intracellular cytokine staining. For cellular composition determination, cells were stained immediately ex vivo after processing or after thawing. Antibody and tetramer information for each flow cytometry panel is listed in Supplementary Data 8–11. Generally, cells were stained as follows (not all steps apply to all panels, all are at room temperature): Washed twice with PBS/BSA (0.1%); 20-min incubation with rhesus MRI tetramer⁴⁹ (NIH Tetramer Core Facility) in PBS/BSA; washed twice with PBS; live/dead stain in PBS for 20 min; washed twice with PBS/BSA; 10-min incubation with human Fc γ blocking reagent (Miltenyi Biotec); incubation with surface marker antibody cocktail in PBS/BSA containing 1 \times Brilliant Stain Buffer Plus (BD Biosciences) for 20 min; washed three times with PBS/BSA (0.1%); 20 min incubation BD Cytotfix/Cytoperm Solution (BD Biosciences); washed twice with Perm/Wash Buffer (BD Biosciences); 30 min incubation with intracellular antibody cocktail in Perm/Wash Buffer containing 1 \times Brilliant Stain Buffer Plus; washed thrice with Perm/Wash Buffer. For Ki-67 staining, samples were stained for surface markers and cytokines as described above, followed by nuclear permeabilization using eBioscience Foxp3/Transcription Factor Staining Buffer (ThermoFisher Scientific) and incubation with antibody against Ki-67 following kit instructions. Data were acquired on either a modified BD LSR II or modified BD FACSymphony and analysed using FlowJo software (v.9.9.6 BD Biosciences). Gating strategies can be found in Supplementary Data 8–11. All cytokine data presented graphically are background-subtracted.

Intravascular CD45 staining

One month after BCG vaccination, macaques in each cohort 6 ($n = 2$ macaques per group) received an IV injection of Alexa Fluor 647-conjugated anti-CD45 antibody (ivCD45; 60 μ g kg⁻¹, clone MB4-6D6, Miltenyi Biotec) 5 min before euthanasia. Blood was collected before anti-CD45 injection as a negative control, and before euthanasia as a positive control. NHPs underwent whole body perfusion with cold

saline before tissue collection. Tissues were processed for BCG CFU quantification and flow cytometric analysis as described above. Staining panels used were as in Supplementary Data 9, with the omission of the APC-conjugated antibodies.

Immunohistochemistry

Embedded tissue sections were deparaffinized (100% xylene, 10 min; 100% ethanol, 5 min; 70% ethanol, 5 min), boiled under pressure for 6 min in antigen retrieval buffer (1 \times Tris EDTA, pH 9.0), and cooled. Sections were blocked in PBS (1% BSA) in a humidified chamber at room temperature for 30 min followed by staining for CD3 (CD3-12, Abcam), CD11c (5D11, Leica), and CD20 (Thermo Scientific, RB-9013-PO) for 18 h at 4 °C in a humidified chamber. After washing with PBS in coplin jars, sections were incubated for 1 h at room temperature with conjugated anti-rabbit IgG Alexa Fluor 488 (Life Technologies, A21206), anti-rat IgG Alexa Fluor 546 (Invitrogen, A11081), and anti-mouse IgG Alexa Fluor 647 (Jackson ImmunoResearch, 75606-150). After washing, coverslips were applied using Prolong Gold anti-fade with Dapi mounting media (Life Technologies). Slides were cured for 18–24 h before imaging on an Olympus FluoView FV1000 confocal microscope. Lung sections were imaged and two random representative 1 mm² ROIs from each macaque were analysed using CellProfiler v2.2.0. Pipelines were designed for analysis by adding modules for individual channel quantification based on pixel intensity and pixel size providing a numerical value for each cell type and total cells. Histological analyses were performed by a veterinary pathologist (E.K.) in a blinded fashion on H&E-stained sections from all tissues obtained.

ELISpot and Luminex

IFN γ ELISpots were performed at 0, 4, 6 and 8 weeks after Mtb and at necropsy. One day before use, hydrophobic high protein binding membranes 96-well plates (Millipore Sigma) were hydrated with 40% ethanol, washed with sterile water, and coated with anti-human/monkey IFN γ antibody (15 μ g ml⁻¹, MT126L, MabTech) overnight at 4 °C. Plates were washed with HBSS and blocked with RPMI with 10% human AB serum for 2 h at 37 °C with 5% CO₂. Approximately 200,000 PBMCs per well were incubated in RPMI supplemented with L-glutamate, HEPES and 10% human AB serum containing 2 μ g ml⁻¹ ESAT-6 or CFP-10 peptide pools for 40–48 h at 37 °C with 5% CO₂. Medium alone or phorbol 12,13-dibutyrate (12.5 μ g ml⁻¹) plus ionomycin (37.5 μ g ml⁻¹) were added as negative (background) and positive controls, respectively. To develop, plates were washed with PBS and biotinylated anti-human IFN γ antibody (2.5 μ g ml⁻¹, 7-B6-1, MabTech) was added for 2 h at 37 °C with 5% CO₂. After washing, streptavidin-horseradish peroxidase (1:100, MabTech) was added for 45 min at 37 °C with 5% CO₂. Spots were stained using AEC peroxidase (Vector Laboratories, Inc.) per the manufacturer's instructions and counted manually on an ELISpot plate reader. Data are reported as average ELISpots from duplicate background-subtracted wells. Wells with confluent spots were described as too numerous to count.

To measure innate cytokine production following BCG immunization, cryopreserved PBMC were batch-analysed. Cells were thawed and resuspended in warm R10. Then, 5×10^5 cells per well in 96-well V-bottom plates were rested overnight at 37 °C with 5% CO₂. Cells were resuspended in Trained Immunity Media¹⁵ plus H37Rv Mtb whole cell lysate (BEI Resources, 20 μ g ml⁻¹), heat-killed *Staphylococcus aureus* (InvivoGen, 1×10^6 per ml), *Escherichia coli* LPS (Sigma-Aldrich, 1 ng ml⁻¹), or RPMI and incubated for 24 h at 37 °C with 5% CO₂ before collecting supernatants. Cytokine and chemokine measurements were determined using a MILLIPLEX NHP cytokine multiplex kit per instructions (Millipore Sigma) and analysed on a Bio-Plex Magpix Multiplex Reader (Bio-Rad).

Antibody ELISAs

IgG, IgA and IgM titres to Mtb H37Rv WCL were assessed in plasma and tenfold concentrated BAL fluid. WCL was used based on greater sensitivity compared to PPD, culture filtrate protein, or lipopolysaccharide.

96-well MaxiSorp ELISA plates (Nunc) were coated overnight at 4 °C with 0.1 µg of WCL. Plates were blocked with PBS/FBS (10%) for 2 h at room temperature and washed with PBS/TWEEN 20 (0.05%). 1:5 serially diluted plasma or concentrated BAL fluid (8 dilutions per sample) was incubated at 37 °C for 2 h, followed by washing. Then, 100 µl of goat anti-monkey HRP-conjugated IgG h+I (50 ng ml⁻¹; Bethyl Laboratories, Inc.), IgA α chain (0.1 µg ml⁻¹, Rockland Immunochemicals Inc.), or IgM α chain (0.4 µg ml⁻¹, Sera Care) was added for 2 h at room temperature, followed by washing. Ultra TMB substrate (100 µl; Invitrogen) was added for 12 min followed by 100 µl 2 N sulfuric acid. Data were collected on a Spectramax i3X microplate reader (Molecular Devices) at 450 nm using Softmax Pro and presented either as endpoint titer (reciprocal of last dilution with an OD above the limit of detection or 2× the OD of an empty well) at 0.2 for IgG and IgA, or midpoint titer for IgM where samples did not titrate to a cut off of 0.2.

Single-cell transcriptional profiling

High-throughput single-cell mRNA sequencing by Seq-Well was performed on single-cell suspensions obtained from NHP BAL, as previously described²⁴. Approximately 15,000 viable cells per sample were applied directly to the surface of a Seq-Well device. At each time point after BCG, two arrays were run for each sample—one unstimulated and one stimulated overnight with 20 µg ml⁻¹ of PPD in R10.

Sequencing and alignment. Sequencing for all samples was performed on an Illumina Nova-Seq. Reads were aligned to the *M. mulatta* genome using STAR⁵⁰, and the aligned reads were then collapsed by cell barcode and unique molecular identifier (UMI) sequences using DropSeq Tools v.1 to generate digital gene expression (DGE) matrices, as previously described^{24,51}. To account for potential index swapping, we merged all cell barcodes from the same sequencing run that were within a hamming distance of 1.

Analysis of single-cell sequencing data. For each array, we assessed the quality of constructed libraries by examining the distribution of reads, genes and transcripts per cell. For each time point, we next performed dimensionality reduction (PCA) and clustering as previously described^{52,53}. We visualized our results in a two-dimensional space using UMAP⁵⁴, and annotated each cluster based on the identity of highly expressed genes. To further characterize substructure within cell types (for example, T cells), we performed dimensionality reduction (PCA) and clustering over those cells alone as previously described²⁴. We then visualized our results in two-dimensional space using *t*-distributed stochastic neighbour embedding (*t*-SNE)²⁴. Clusters were further annotated (that is, as CD4 and CD8 T cells) by cross-referencing cluster-defining genes with curated gene lists and online databases (that is, SaVanT and GSEA/MsigDB)^{55–57}.

Module identification. Data from stimulated or unstimulated T cells at week 13 or 25 was subset on significant principal components as previously described²⁴ and, for those principal components, on genes with significant loadings as determined through a randomization approach ('JackStraw')⁵². These matrices were then used as the inputs for WGCNA⁵⁸. Following the WGCNA tutorial (<https://horvath.genetics.ucla.edu/html/CoexpressionNetwork/Rpackages/WGCNA/Tutorials/>), we chose an appropriate soft power threshold to calculate the adjacency matrix. As scRNA-seq data is affected by transcript drop-out (failed capture events), adjacency matrices with high power further inflate the effect of this technical limitation, and yield few correlated modules. Therefore, when possible, we chose a power as suggested by the authors of WGCNA (that is, the first power with a scale free topology above 0.8); however, if this power yielded few modules (fewer than three), we decreased our power. We then generated an adjacency matrix using the selected soft power and transformed it into a topological overlap matrix (TOM). Subsequently, we hierarchically clustered this

TOM, and used the `cutreeDynamic` function with method 'tree' to identify modules of correlated genes using a dissimilarity threshold of 0.5 (that is, a correlation of 0.5). To test the significance of the correlations observed in each module, we implemented a permutation test. Binning the genes in the true module by average gene expression (number of bins = 10), we randomly picked genes with the same distribution of average expression from the total list of genes used for module discovery 10,000 times. For each of these random modules, we performed a one-sided Mann–Whitney *U*-test between the distribution of dissimilarity values among the genes in the true module and the distribution among the genes in the random module. Correcting the resulting *P* values for multiple hypothesis testing by Benjamini–Hochberg false discovery rate correction, we considered the module significant if fewer than 500 tests (*P* < 0.05) had false discovery rate > 0.05.

Gene module enrichments. To characterize the seven significant gene modules identified among in vitro-stimulated T cells collected 13 weeks after vaccination, we performed an enrichment analysis using databases of gene expression signatures (SaVanT and GSEA/MsigDB). Specifically, the enrichments in the Savant database, which includes signatures from ImmGen, mouse body atlas and other datasets (<http://newpathways.mcdb.ucla.edu/savant-dev/>), were performed using genes included in significant modules with a background expression set of 32,681 genes detected across single cells using Piano (<https://varemo.github.io/piano/>).

Statistical methods

All reported *P* values are from two-sided comparisons. For continuous variables, vaccine routes were compared using a Kruskal–Wallis test with Dunn's multiple comparison adjustment or one-way ANOVA with Dunnett's multiple comparison adjustment (comparing all routes to ID_{low} BCG). Fisher's exact tests were run for multiple CFU thresholds (evaluating protection) to assess the association between vaccine route and protection from Mtb (Extended Data Fig. 8b). A permutation test⁵⁹ was used to compare fractional distributions (pie charts) of all vaccine groups to ID_{low} BCG. For clinical parameters, combined pre-vaccination measurements from all NHPs were compared against distributions from every vaccine group at every time point using Dunnett's test for multiple comparisons. To assess whether post-vaccination antigen-responsive CD4 or CD8 T cells in the BAL or PBMCs are associated with disease severity, we first calculated peak T cell responses for each NHP over the course of vaccine regimen. The log₁₀-transformed CD4 and CD8 cell counts were calculated within BAL and frequencies of CD4 and CD8 cells were calculated within PBMCs. To assess the effects of vaccine route and T cells on log₁₀-transformed total CFUs, several multiple linear regressions were run in JMP Pro (v.12.1.0). Peak T cell responses and CFUs for each macaque included in these analyses are provided in Supplementary Table 1; detailed regression output (including model fit, ANOVA results, effect tests and parameter estimates) is provided in Supplementary Table 5. Cytokine production for trained immunity assay was compared using a two-way ANOVA and Dunnett's multiple comparison test. Serial PBMC responses to CFP, ESAT-6 or CFP-10 by IFNγ ELISpot were analysed by using a Wilcoxon signed-rank test to compare pre-infection versus 12 weeks post-infection time points (within each vaccine route).

Reporting summary

Further information on research design is available in the Nature Research Reporting Summary linked to this paper.

Data availability

All relevant data are available from the corresponding author upon reasonable request. Supplementary Table 1 provides peak immune data and post-challenge data for individual NHPs and Supplementary Table 5

Article

provides regression analyses that support Extended Data Fig. 13. Supplementary Tables 2–4 include stimulation-inducible module genes, gene enrichments for modules, and differentially expressed genes that support transcriptional profiling data. RNA-sequencing data that support this study have been deposited in the Gene Expression Omnibus (GEO) under accession number GSE139598. Source Data for Figs. 1–4 and Extended Data Figs. 2–13 are provided with the paper.

Code availability

All R code used for analysis of Seq-Well data is available upon request.

42. Fitzpatrick, M. et al. Comparison of pellicle and shake flask-grown BCG strains by quality control assays and protection studies. *Tuberculosis (Edinb.)* **114**, 47–53 (2019).
43. Saini, D. et al. Ultra-low dose of *Mycobacterium tuberculosis* aerosol creates partial infection in mice. *Tuberculosis (Edinb.)* **92**, 160–165 (2012).
44. Martin, C. J. et al. Digitally barcoding *Mycobacterium tuberculosis* reveals in vivo infection dynamics in the macaque model of tuberculosis. *mBio* **8**, e00312-17 (2017).
45. Coleman, M. T. et al. Early changes by ¹⁸F-fluorodeoxyglucose positron emission tomography coregistered with computed tomography predict outcome after *Mycobacterium tuberculosis* infection in cynomolgus macaques. *Infect. Immun.* **82**, 2400–2404 (2014).
46. Lin, P. L. et al. Sterilization of granulomas is common in active and latent tuberculosis despite within-host variability in bacterial killing. *Nat. Med.* **20**, 75–79 (2014).
47. White, A. G. et al. Analysis of ¹⁸F-DG PET/CT imaging as a tool for studying *Mycobacterium tuberculosis* infection and treatment in non-human primates. *J. Vis. Exp.* **127**, e56375 (2017).
48. Phuah, J. et al. Effects of B cell depletion on early *Mycobacterium tuberculosis* infection in cynomolgus macaques. *Infect. Immun.* **84**, 1301–1311 (2016).
49. Corbett, A. J. et al. T-cell activation by transitory neo-antigens derived from distinct microbial pathways. *Nature* **509**, 361–365 (2014).
50. Dobin, A. et al. STAR: ultrafast universal RNA-seq aligner. *Bioinformatics* **29**, 15–21 (2013).
51. Macosko, E. Z. et al. Highly parallel genome-wide expression profiling of individual cells using nanoliter droplets. *Cell* **161**, 1202–1214 (2015).
52. Satija, R., Farrell, J. A., Gennert, D., Schier, A. F. & Regev, A. Spatial reconstruction of single-cell gene expression data. *Nat. Biotechnol.* **33**, 495–502 (2015).
53. Wolf, F. A., Angerer, P. & Theis, F. J. SCANPY: large-scale single-cell gene expression data analysis. *Genome Biol.* **19**, 15 (2018).
54. Becht, E. et al. Dimensionality reduction for visualizing single-cell data using UMAP. *Nat. Biotechnol.* **37**, 38–44 (2018).
55. Lopez, D. et al. SaVanT: a web-based tool for the sample-level visualization of molecular signatures in gene expression profiles. *BMC Genomics* **18**, 824 (2017).
56. Mootha, V. et al. PGC-1 α -responsive genes involved in oxidative phosphorylation are coordinately downregulated in human diabetes. *Nat. Genet.* **34**, 267–273 (2003).
57. Subramanian, A. et al. Gene set enrichment analysis: a knowledge-based approach for interpreting genome-wide expression profiles. *Proc. Natl Acad. Sci. USA* **102**, 15545–15550 (2005).

58. Langfelder, P. & Horvath, S. WGCNA: an R package for weighted correlation network analysis. *BMC Bioinformatics* **9**, 559 (2008).
59. Roederer, M., Nozzi, J. L. & Nason, M. C. SPICE: exploration and analysis of post-cytometric complex multivariate datasets. *Cytometry A* **79**, 167–174 (2011).

Acknowledgements This project was funded by the Intramural Research Program of the VRC, NIAID, NIH and by the Bill and Melinda Gates Foundation (through Aeras to J.L.F. and to A.K.S.). A.K.S. was also supported, in part, by the Searle Scholars Program, the Beckman Young Investigator Program, the NIH (5U24AI118672, 2RM1HG006193), and a Sloan Fellowship in Chemistry. We acknowledge the outstanding work of veterinary and research technicians (J. Tomko, B. Stein, C. Ameel, A. Myers, N. Schindler, C. Cochran and C. Bigbee), and imaging personnel (L. J. Frye, J. Borish) at the University of Pittsburgh, as well as attending veterinarian D. Scorpio and animal program coordinators J. P. Todd, A. Taylor and H. Bao at the VRC, and BioQual, Inc. for expert animal care. We thank Flynn, Seder and Roederer laboratory members for discussions, Aeras members M. Fitzpatrick and J. Schaeffer for assistance with BCG, VRC NHP Immunogenicity Core for technical assistance, and VRC Flow Cytometry Core members for support. We are grateful to PARI Pharma GmbH for providing the eFlow nebulizer for use in this study.

Author contributions R.A.S., M.R. and J.L.F., conceived and designed experiments with P.A.D., D.J.L., A.K.S., C.A.S., D.C. and A.B. Pre-challenge data was generated at the NIH Vaccine Research Center under guidance of R.A.S. and M.R., who helped to write manuscript; P.A.D. wrote animal protocols, coordinated immunizations and NHP sampling, processed samples, designed flow cytometry panels (with M.R.), performed flow cytometry and analysis, created figures and helped write the manuscript. J.A.H. helped to develop staining panels, performed flow cytometry and analysis; M.H.W. and T.K.H. performed Seq-Well assays and transcriptional profiling analyses, and created figures with A.K.S., who helped to write the manuscript. S.P. performed antibody assays, BCG quantification in tissues, and flow cytometry with M.K.; P.A.S. performed PBMC adaptive and trained immunity assays and analysis. Post-challenge data were generated at the University of Pittsburgh under the oversight of J.L.F., who helped to write the manuscript; C.A.S. wrote animal protocols and coordinated all animal challenge experiments; J.J.Z. and M.A.R. processed samples and assessed immunology and microbiology post-challenge and performed data analysis; N.L.G. performed immunohistochemistry; C.M.C., P.L.L., E.K., J.L.F. and J.J.Z. performed animal procedures, necropsies and sample processing; P.M. and A.G.W. performed PET–CT scan, data and statistical analyses; J.J.Z. and P.M. generated figures from analysed data.

Competing interests Authors from University of Pittsburgh, NIH and MIT have no competing interests. A.B. is currently an employee of Vir Biotechnology, Inc., which is developing a CMV-based vaccine candidate for TB.

Additional information

Supplementary information is available for this paper at <https://doi.org/10.1038/s41586-019-1817-8>.

Correspondence and requests for materials should be addressed to R.A.S.

Peer review information *Nature* thanks Joel Ernst, Stefan Kaufmann and the other, anonymous, reviewer(s) for their contribution to the peer review of this work.

Reprints and permissions information is available at <http://www.nature.com/reprints>.

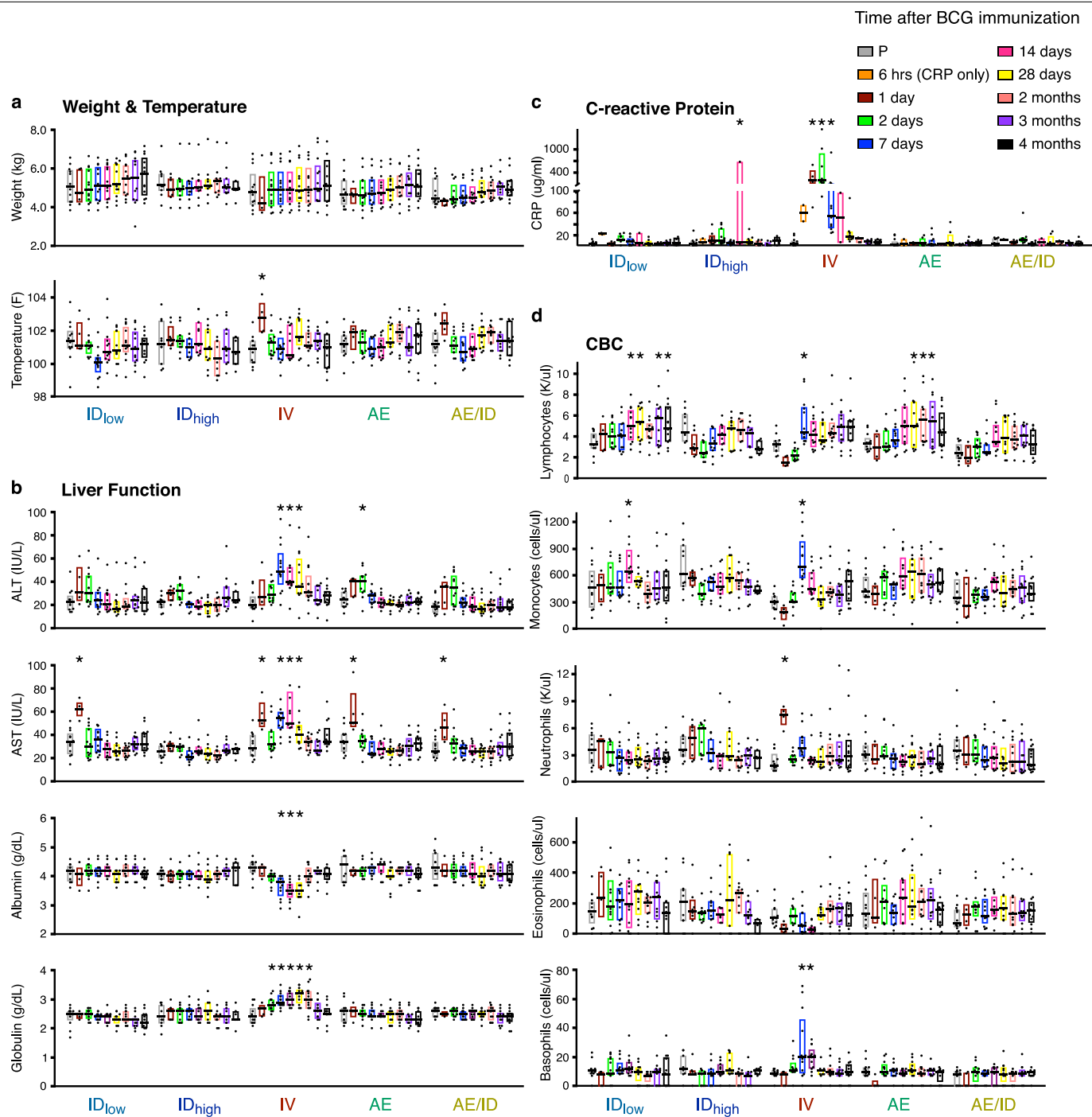
Group	Vaccine	BCG Route	Target Dose (CFU)	# of NHP Challenged
1	ID _{low}	Intradermal (1 site)	5x10 ⁵	10
2	ID _{high}	Intradermal (2 sites)	5x10 ⁷	8
3	IV	Intravenous	5x10 ⁷	10
4	AE	Aerosol	5x10 ⁷	10
5	AE/ID	Aerosol/Intradermal	5x10 ⁷ /5x10 ⁵	10
6	Unvax	Unvaccinated	N/A	4

Study Week	Pre	0	4	8	12	16	20	24	28	32	36
BCG vaccination											
PBMC collection											
BAL collection											
Mtb challenge											
PET CT scan											
Necropsy											

	Cohort	BCG Dose (CFU)			Duration	Challenge	Number of Macaques Per Arm							Total
		Low Dose ID	High Dose ID	High Dose IV, AE, EB			Time to Challenge (Weeks)	Mtb Dose (CFU)	ID low (n)	ID high (n)	IV (n)	AE (n)	AE/ID (n)	
Immunology & Challenge	1	3.5x10 ⁵	-	5.2x10 ⁷	27	4	3	-	2	3	2	-	-	10
					29	16	2	-	3	2	3	-	-	10
	2	3.1x10 ⁵	2.9x10 ⁷	3.7x10 ⁷	22/26	8	2	2	2	2	-	-	10	
					24/28	11	2	2	2	2	-	-	10	
	3	3.1x10 ⁵	2.9x10 ⁷	3.7x10 ⁷	37/41	16	0	2	1	0	1	-	2	6
					38/42	36	1	2	0	1	0	-	2	6
Immunology Only	4	2.1x10 ⁶	4.7x10 ⁷	3.7x10 ⁷	N/A	N/A	3	3	3	3	3	-	-	15
	5a	1.6x10 ⁵	1.9x10 ⁷	2.5x10 ⁷	N/A	N/A	1	1	1	-	1	-	-	4
	5b	2.2x10 ⁶	2.2x10 ⁷	1.2x10 ⁷	N/A	N/A	1	1	1	-	1	-	-	4
	5c	1.5x10 ⁶	4.3x10 ⁷	2.4x10 ⁷	N/A	N/A	2	2	2	2	-	-	-	8
ivCD45	6	-	7.4x10 ⁷	3.6x10 ⁷	N/A	N/A	-	2	2	2	-	2	-	8
		BCG Dose (CFU)												
		Low Dose ID		High Dose IV or AE	Medium Dose IV or AE	Low Dose AE								
Immunology Pilot	Pilot a	3.7x10 ⁵		5.6x10 ⁶ (AE)	5.7x10 ⁴ (AE)	6.0x10 ²	3	-	-	-	9	-	-	12
	Pilot b	-		2.1x10 ⁷ (AE)	2.7x10 ⁵ (AE)	-		-	-	6	-	-	-	6
	Pilot c	-		3.5x10 ⁷ (IV)	5.8x10 ⁵ (IV)	-	-	-	6	-	-	-	-	6
	NHP (BCG or Unvax)						20	17	25	23	24	2	4	115
	NHP (TB Challenge)						10	8	10	10	10		4	52

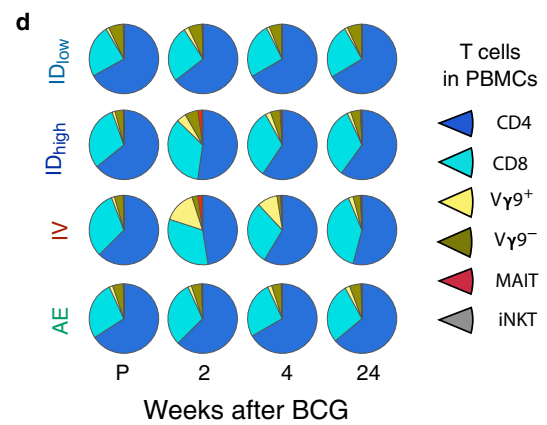
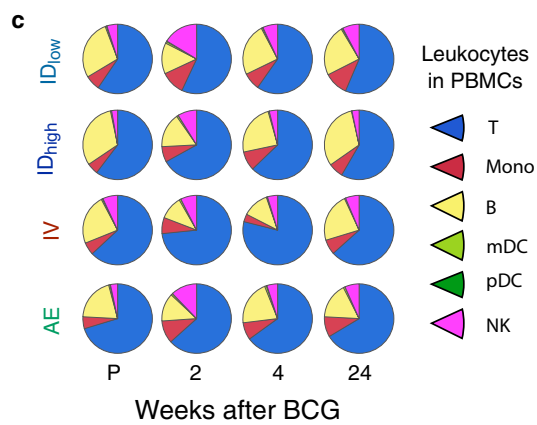
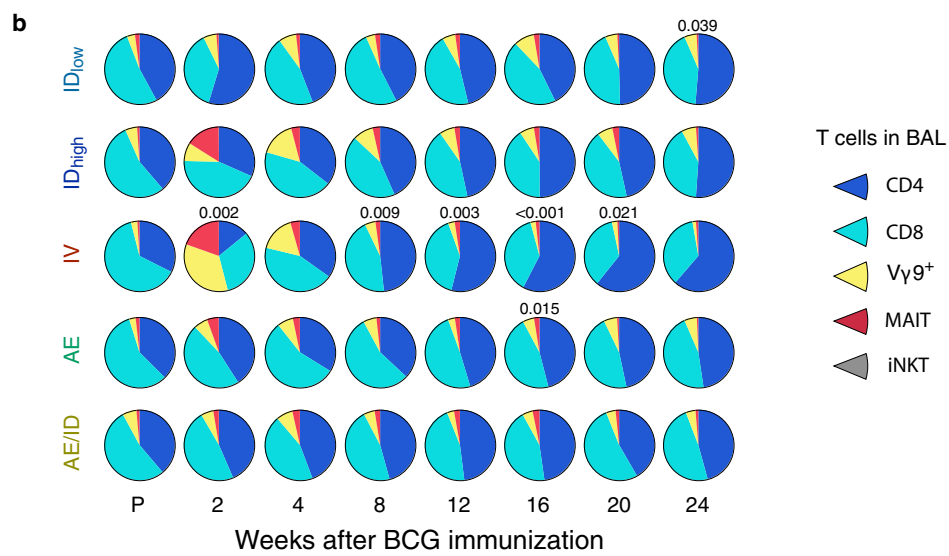
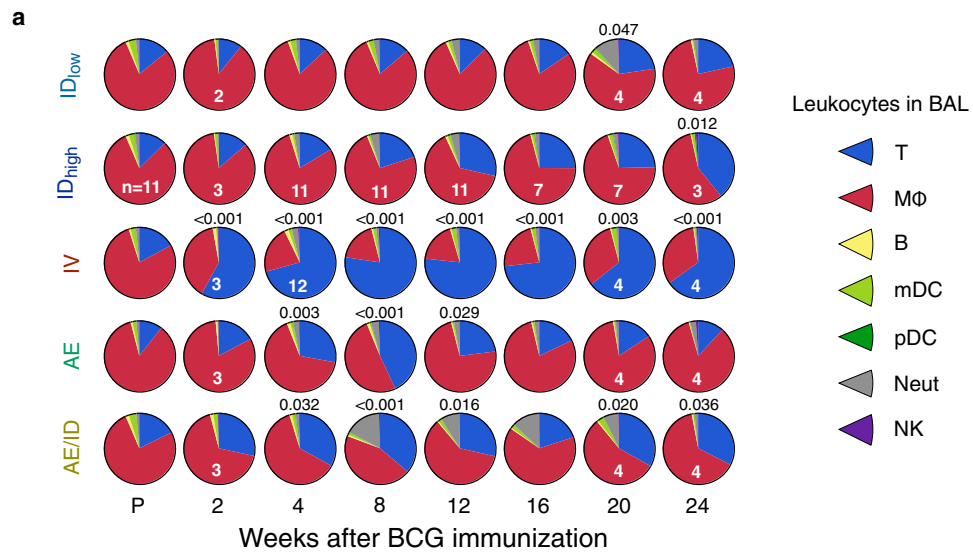
Extended Data Fig. 1 | Study design, vaccine regimens, macaques and cohorts. **a**, Vaccine groups including route of BCG administration, target dose of BCG to be delivered (CFUs), and number of NHPs per BCG regimen (*n* = 10 macaques except ID_{high}, *n* = 8 macaques). Note that ID_{low} and ID_{high} groups received BCG in one or two sites, respectively, and AE/ID group received AE (high-dose) and ID (low-dose) BCG simultaneously. Unvaccinated macaques (*n* = 4) were used as Mtb challenge controls. **b**, Timeline for Mtb challenge cohorts including weeks relative to BCG vaccination for PBMC and BAL sample collection, Mtb challenge, PET–CT scanning, and scheduled necropsy after challenge. Macaques that met humane end-point criteria were euthanized earlier than 12 weeks post-challenge (Supplementary Table 1). **c**, Data are from a total of 115 rhesus macaques, 52 of which were challenged with Mtb. Owing to the ABSL-3 capacity constraints and logistical limits in the number of macaques that can be sampled, scanned by PET–CT, or necropsied at any given time point, studies were broken into sequentially immunized and/or challenged cohorts. A maximum of 20 NHPs were infected with Mtb in any challenge cohort with infections split over 2 days, staggered by 2 weeks. The actual doses of BCG administered, determined by subsequent culture, is noted for each vaccine group. The time interval between vaccination and challenge is noted in weeks

and the challenge dose of Mtb (CFUs) is listed for each challenge cohort (BCG vaccine dose and Mtb challenge dose for individual NHPs, along with peak immune responses and detailed outcome data, is provided in Supplementary Table 1). Protection data are from 8–10 BCG-immunized NHPs per group and 4 unvaccinated controls in cohorts 1–3 (‘Immunology & challenge’). Per protocol, BAL samples were not collected from animals 8 weeks before, or after, Mtb challenge. Three NHPs per vaccine group were immunized just as in cohorts 1–3 but were not challenged. Instead, these macaques (cohort 4; ‘Immunology only’) were sampled (BAL, PBMC) for 6 months after BCG immunization and then euthanized to perform extensive immune analysis in various tissues at what would have been the time of challenge. BAL samples from cohort 4 were transcriptionally profiled at weeks 13 and 25. Cohort 5 (a–c) includes 4 macaques per group (except AE and AE/ID groups, *n* = 2 NHPs each) that were immunized with BCG and were euthanized 1–3 months later to assess BCG CFUs and T cell responses in various tissues. NHPs in cohort 6 (‘ivCD45’, *n* = 2 macaques per group) received anti-CD45 injection before necropsy to distinguish blood- and tissue-derived cells. Pilot cohorts (a–c) include NHPs enrolled in the dose-finding pilot study (*n* = 3 macaques per dose and route; ‘Immunology pilot’).



Extended Data Fig. 2 | Clinical parameters after BCG vaccination in NHPs. To assess safety of BCG vaccinations, all macaques (cohorts 1–4 excluding unvaccinated) were monitored for changes in several clinical parameters at various time points after BCG. After vaccination, changes were observed predominantly in IV BCG macaques; however, all were transient. **a**, Weight and temperature: there was a 0.9 °C increase in body temperature in the IV BCG group at day 1, which resolved by day 2; the average pre-vaccination temperature across all NHPs was 38.4 °C. **b**, Liver function tests (alanine aminotransferase (ALT), aspartate aminotransferase (AST), albumin and globulin): there was a twofold increase in ALT and AST above pre-vaccination levels (20–30 IU l⁻¹) in the IV BCG group, which resolved by day 28. **c**, C-reactive protein (CRP) in the IV BCG group increased up to a median of 400 µg ml⁻¹ at day 2, which resolved by day 14; the average pre-vaccination CRP level in plasma

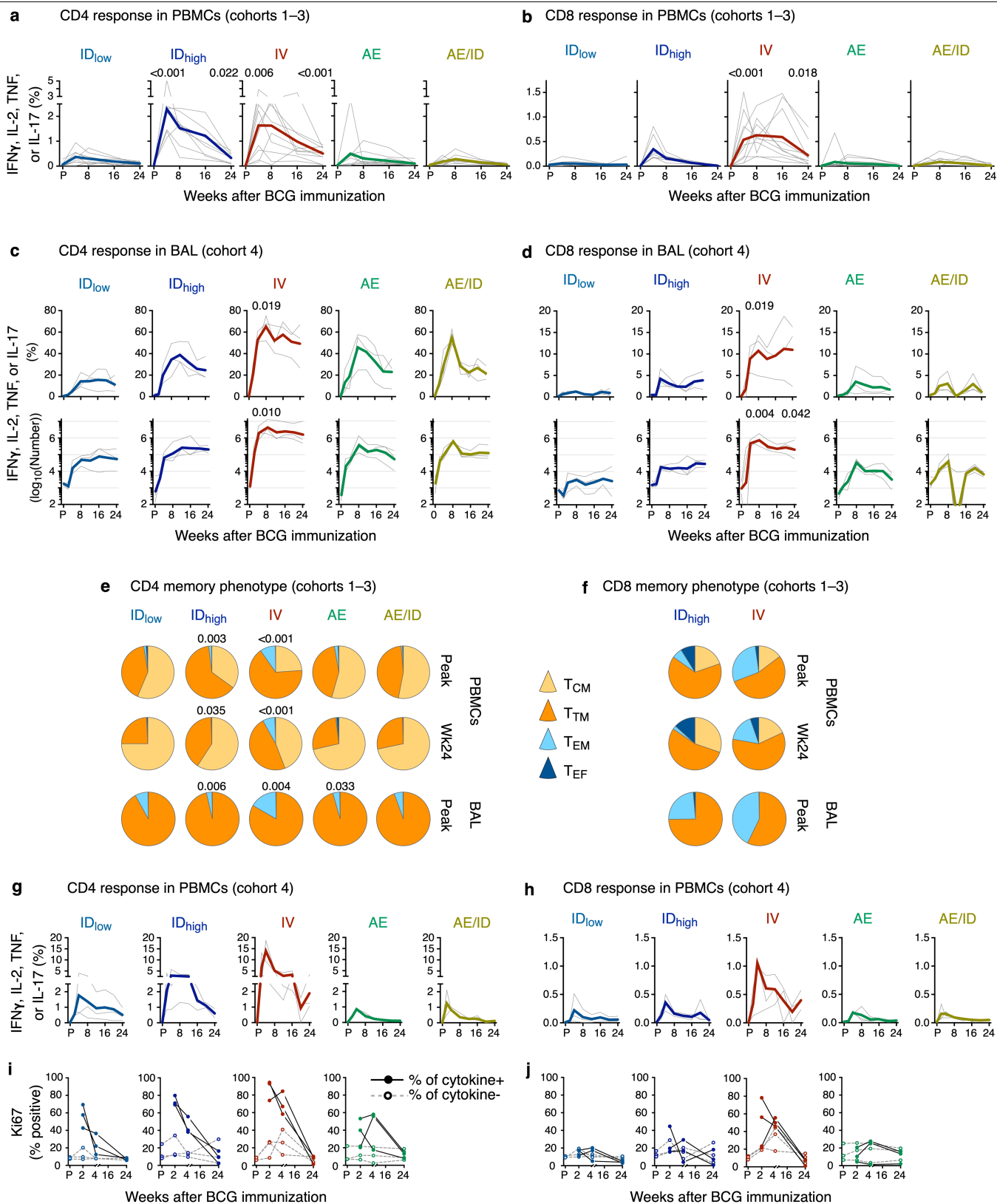
across all NHPs ranged from 0 to 28 µg ml⁻¹. **d**, Complete blood counts (CBC). Transient increases in numbers of circulating neutrophils (day 1) and lymphocytes, monocytes and basophils (day 7) were observed in the IV BCG group. All tests were performed longitudinally on whole blood at time of collection except CRP, which was batch-analysed from frozen plasma samples; the 6-h time point was measured for CRP only. Data points shown are individual NHPs ($n = 11–13$ per group, $n = 63$ total) with interquartile range (box) and median (line). For each parameter, pre-vaccination (P) measurements for all NHPs were combined and compared against distributions from every vaccine group at every time point using Dunnett's test for multiple comparisons; * $P < 0.05$. No clinical signals, such as lethargy, appetite suppression or weight loss, were observed up to time of Mtb challenge, 24 weeks later.



Extended Data Fig. 3 | See next page for caption.

Extended Data Fig. 3 | Proportions of leukocyte and T cell subsets in the BAL and PBMCs after BCG immunization. a–d. We assessed whether the composition of leukocytes in the BAL or PBMCs was altered after BCG vaccination. Shown are pie graphs comprising proportions of indicated leukocytes (**a, c**) or CD3⁺ T cell subsets (**b, d**) in BAL (**a, b**) and PBMCs (**c, d**) for each BCG regimen from pre-vaccination up to 24 weeks post-BCG, identified using multi-parameter flow cytometry as in Supplementary Data 8. **a**, In the BAL, the rapid and sustained increase in T cell (but not macrophage) number (Fig. 1a and Supplementary Data 2b) altered the overall cellular composition of BAL from approximately 75% alveolar macrophages (red) and 15% T cells (blue) before vaccination to approximately 65% T cells and 30% macrophages, even 6 months after IV BCG. **b**, To delineate the composition of BAL T cells further, the proportions of CD4 and CD8 T cells, as well as non-classical T cells ($\gamma\delta$, MAIT and iNKT) that may also have a role in protection against TB^{9–11} were assessed.

Two weeks after vaccination, there was a substantial but transient increase in the proportion of V γ 9⁺ $\gamma\delta$ T cells and MAIT cells after IV BCG, and a trend towards increased V γ 9⁺ $\gamma\delta$ T cells and MAIT cells after BCG ID_{high}. However, by 8 weeks, the proportions of these non-classical T cells contracted to pre-vaccination levels. **c, d**, A similar analysis was performed to determine how the route of BCG immunization influenced the composition of leukocytes in PBMCs. Here, IV BCG induced a transient increase in V γ 9⁺ $\gamma\delta$ T cells but not MAIT cells. BAL pie graphs represent the average proportions from 13 NHPs per BCG regimen (cohorts 1–4; Extended Data Fig. 1c) except where indicated (white numbers in **a** also apply to **b**). PBMC pie graphs represent the average proportions from three NHPs per BCG regimen (cohort 4). B, B cells; M ϕ , macrophages; Mono, monocytes; T, T cells; Neut, neutrophils. *P* values indicate differences compared to pre-vaccination within the same vaccine group using a Permutation test.



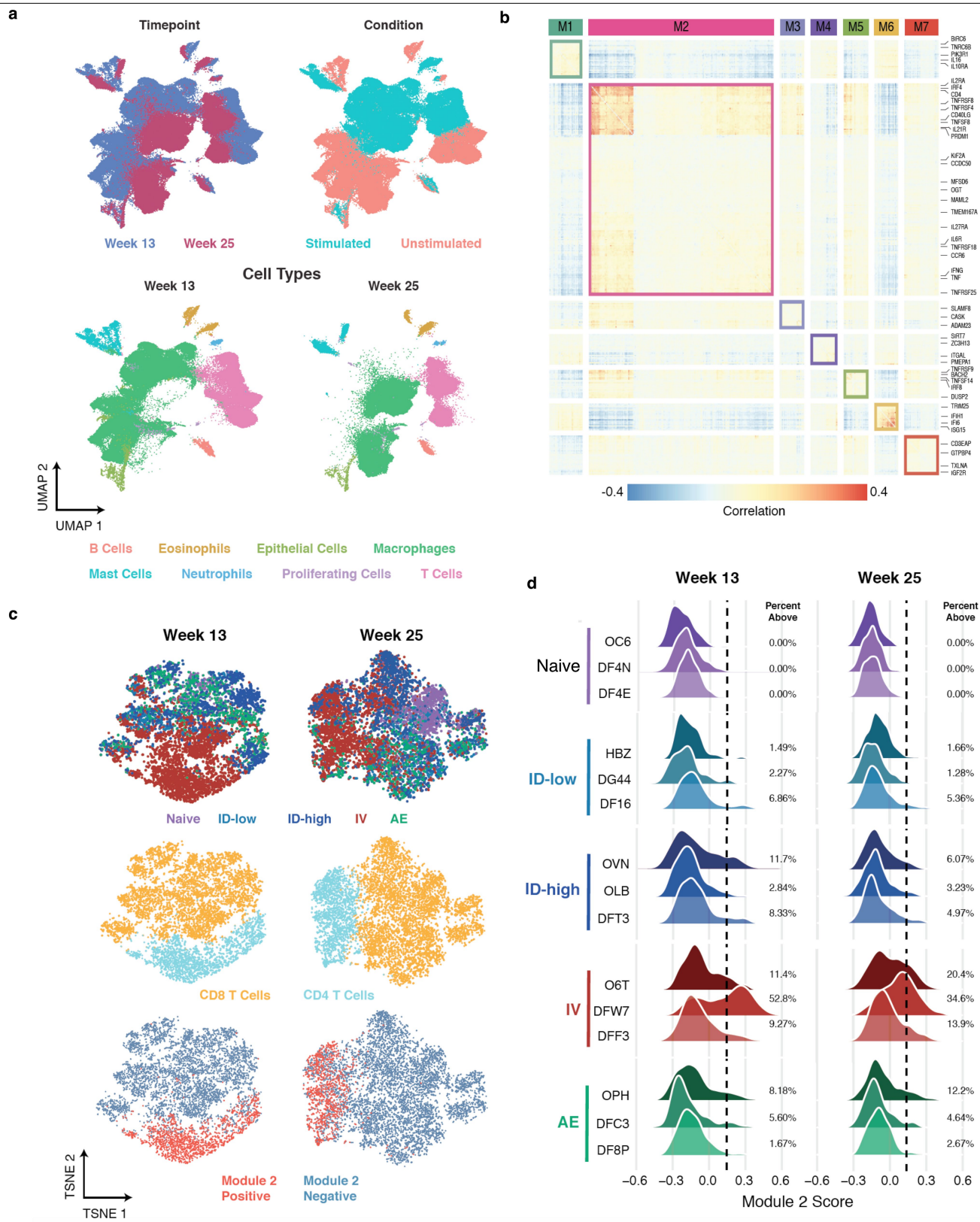
Extended Data Fig. 4 | See next page for caption.

Extended Data Fig. 4 | Extended immune data from challenge and immunology cohorts. **a, b**, Full kinetics of PBMC responses from NHPs in challenge cohorts (cohorts 1–3, $n = 8–11$ macaques) as in Fig. 1b, c. Shown is the frequency of memory CD4 (**a**) or CD8 (**b**) T cells producing any combination of IFN γ , IL-2, TNF or IL-17 in response to PPD stimulation at various time points before and up to 24 weeks after BCG. Grey lines are individual NHP responses; bold, coloured lines represent the median response. Each group was compared to ID $_{low}$ at weeks 4 and 24 (one-way ANOVA; P values are Dunnett's multiple comparison test). **c, d**, T cell responses from a replicate cohort of similarly BCG-immunized rhesus macaques (cohort 4, $n = 3$ NHPs) from which BAL was collected for 24 weeks after BCG vaccination. Shown is the frequency (top) or absolute number (log $_{10}$ -transformed; bottom) of CD4 (**c**) or CD8 (**d**) memory T cells expressing any combination of IFN γ , IL-2, TNF or IL-17 in response to PPD stimulation, before and up to 24 weeks after BCG vaccination. Kruskal–Wallis test was used to compare each group to ID $_{low}$ at weeks 8 (peak) and 24 (time of challenge); P values are Dunn's multiple comparison test. **e, f**, The memory phenotype of antigen-responsive CD4 (**e**) and CD8 (**f**) T cells in PBMCs and BAL at the peak of the response (week 4 for PBMC, week 8–12 for BAL; cohorts 1–3, $n = 8–10$ macaques) and time of challenge (week 24 collected for PBMC only) was assessed. Cytokine-positive T cells from PBMCs were categorized as central memory (T $_{CM}$), T $_{TM}$, effector memory (T $_{EM}$), or terminal effectors (T $_{EF}$) based on expression of CD45RA, CD28 and CCR7 as shown in Supplementary

Data 10. Most responding cells in PBMCs were central memory and transitional memory T cells, with the proportion of transitional memory cells greater in ID $_{high}$ - and IV-BCG-immunized NHPs compared with the ID $_{low}$ group. In BAL, where T cells are CCR7-negative, most responding CD4 T cells were CD45RA $^{+}$ CD28 $^{+}$ T $_{TM}$ cells (Supplementary Data 9). For CD8 memory phenotypes, pie graphs are shown only for groups that displayed measurable frequencies of cytokine $^{+}$ CD8 T cells. IV-BCG-immunized NHPs had larger proportions of T $_{EM}$ cells in PBMCs and BAL, which suggests a more diverse composition of memory and effector cells than other routes. P values indicate differences compared to ID $_{low}$ using a permutation test (CD4 pie graphs only). **g–j**, PBMC T cell responses from a replicate cohort of similarly BCG-immunized rhesus macaques (cohort 4, $n = 3$ macaques). Shown is the frequency of CD4 (**g**) and CD8 (**h**) memory T cells producing any combination of IFN γ , IL-2, TNF or IL-17 in response to PPD stimulation before and up to 24 weeks after BCG. **i, j**, As an immunological indicator of recent antigen exposure and proliferation due to BCG persistence in vivo, Ki-67 expression in PBMCs over the course of immunization was assessed. Shown is the percentage of cytokine-positive (closed symbols, solid lines) or cytokine-negative (open symbols, dashed lines) memory CD4 or CD8 T cells expressing Ki-67 as identified in Supplementary Data 11. In IV-BCG-immunized NHPs, at least 60% of antigen-responsive CD4 T cells in blood were Ki-67 $^{+}$ at 2 and 4 weeks after BCG but were at baseline 6 months later.

Extended Data Fig. 5 | Quality of T cell responses in PBMCs and BAL after BCG immunization. The composition of the cytokine responses at the single-cell level, or ‘quality’ of the response, can reveal distinct functional differences that associate with protection against Mtb and other pathogens^{19,20}. Here, the quality was defined by the relative proportion of antigen-stimulated cells producing every combination of IFN γ , IL-2 and TNF, with or without CD154 or IL-17. CD154 (also known as CD40L) expression in PBMCs was measured as a sensitive marker for detection of all antigen-stimulated CD4 T cells²¹ based on evidence for CD4-dependent, IFN γ -independent mechanisms of protection against TB^{22,23}. Shown are peak PPD-responsive memory CD4 and CD8 T cell responses in PBMCs (**a**, week 4) or BAL (**b**, week 12) after BCG vaccination for challenge cohorts 1–3 ($n = 8–11$ NHPs); analysis of all time points is shown in Supplementary Data 4 and 5. **a**, Bar graphs show the frequency of T cells in PBMCs expressing CD154 with IFN γ , IL-2, or TNF production, and total IL-17 production (CD4 response, top) or IFN γ , IL-2, or TNF for the CD8 response (bottom). Individual NHP responses are shown with interquartile range (bar

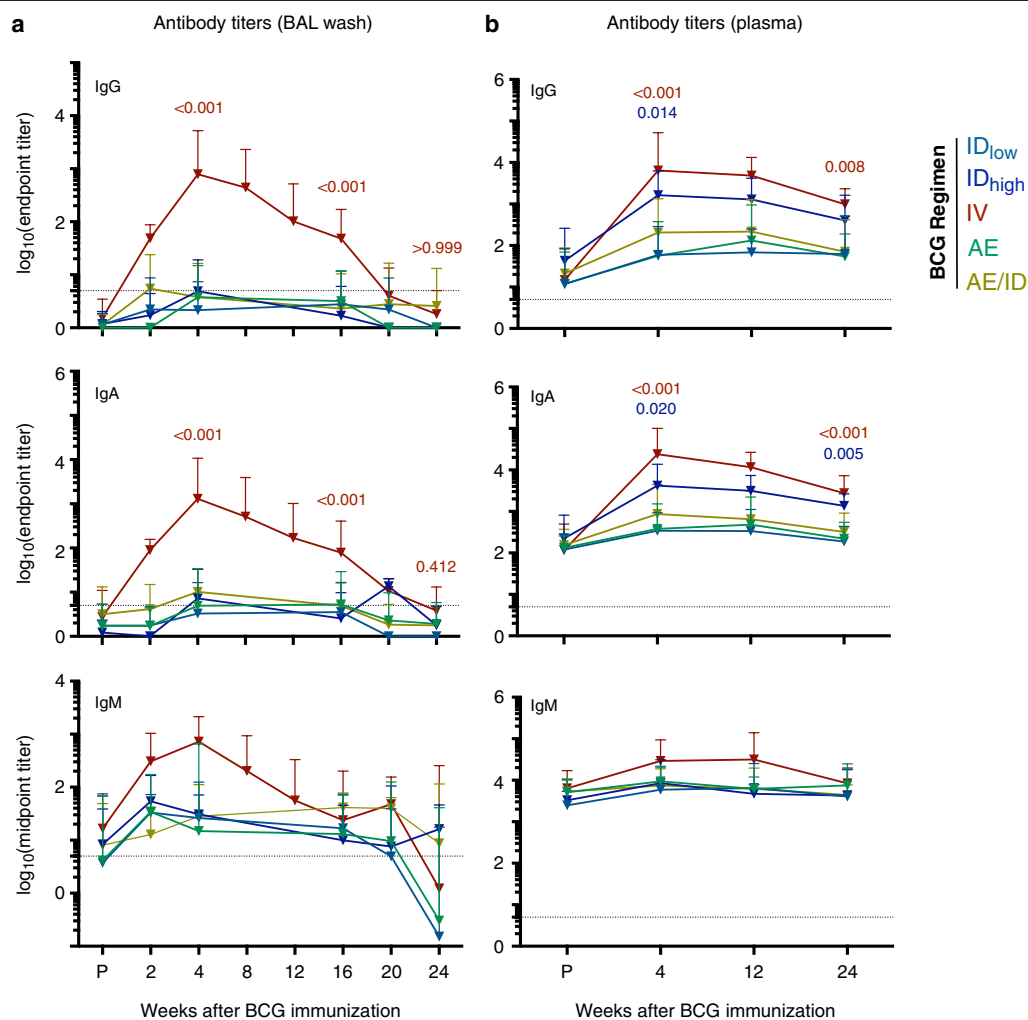
and median (horizontal line)). Pie graphs represent the proportion of the total response comprising each cytokine combination, averaged for all NHPs, and are not shown for groups with low to undetectable responses. The proportion of the response producing IL-17 (with or without other cytokines) is indicated with a black arc and the proportion expressing CD154 alone is the black pie section. **b**, Bar graphs show the frequency of CD4 or CD8 T cells in BAL producing IFN γ , IL-2 or TNF, and total IL-17 production. Pie graphs represent the average proportion of total cytokine production comprising each cytokine combination; the proportion of the total response producing IL-17 (with or without other cytokines) is indicated with a black arc. Despite the notable differences in the magnitude of responses amongst BCG regimens, there were no differences in the quality of CD4 T cell responses nor CD8 T cell responses in PBMC or BAL. Of note, approximately 90% of the CD4 T cell responses were composed of T_H1 cytokines with fewer than 10% also producing IL-17; most IL-17 producing CD4 T cells co-expressed T_H1 cytokines.



Extended Data Fig. 6 | See next page for caption.

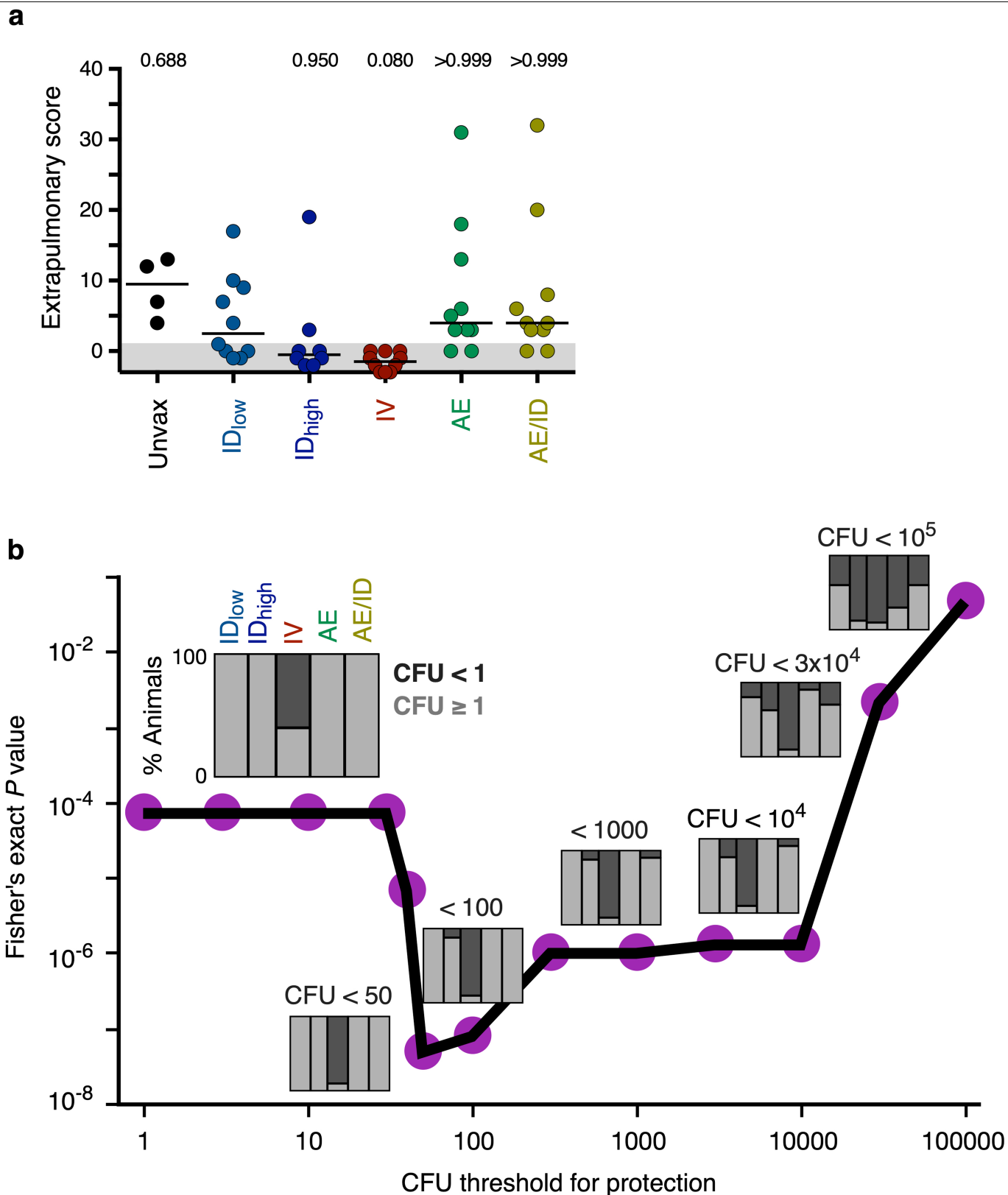
Extended Data Fig. 6 | Identification of gene modules and distribution of module scores. A total of 162,490 single-cell transcriptomes derived from unstimulated and PPD-stimulated BAL cells from 15 NHPs (cohort 4, $n = 3$ per group) at weeks 13 (peak of BAL response) and 25 (time of challenge) were profiled. **a.** Uniform manifold approximation and projection (UMAP) plots of BAL cells at weeks 13 and 25 after BCG immunization, coloured by time point (top left), PPD stimulation condition (top right), and cell type (week 13, bottom left; week 25, bottom right). **b.** Gene–gene correlation heat map showing significant gene modules (M1–M7; top) identified among week 13 stimulated

BAL T cells with select genes (right) highlighted. **c.** t -Distributed stochastic neighbour embedding (t -SNE) plots of stimulated BAL T cells from weeks 13 (left) and 25 (right), coloured by vaccine group (top), T cell subtypes (middle), and module 2-positivity (bottom). **d.** Histograms of the distribution of module 2 scores by vaccine group (colour) and macaque. Dashed line (placed at two s.d. above the mean score in the naive controls) indicates the threshold used to call cells as positive for the module. The percentage module 2-positive is shown for each NHP.



Extended Data Fig. 7 | Humoral immune response in BAL and plasma after BCG immunization. Mtb-responsive antibody responses were assessed in BAL and plasma after BCG immunization. Mtb WCL-specific IgG, IgA and IgM antibody titres were measured from individual NHPs at various time points before and after BCG immunization. Shown are end-point titres for IgG and IgA and mid-point titres for IgM (in which the end point was not reached) **a**, Antibody titres in tenfold-concentrated BAL fluid (cohorts 1–4, $n = 11$ –13 macaques except at weeks 2, 20 and 24, cohort 4 only, $n = 3$ macaques). In

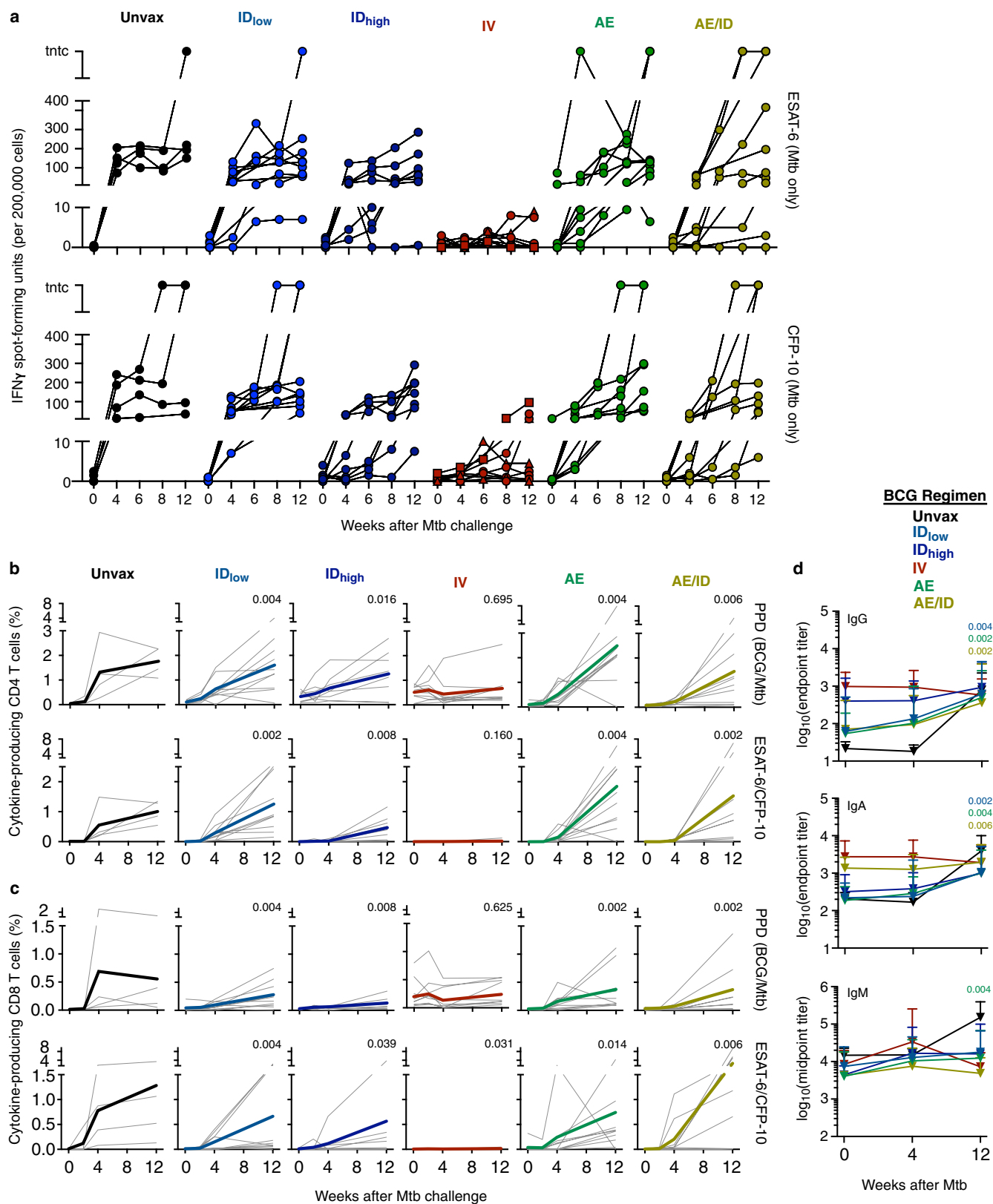
concentrated BAL fluid, antigen-responsive IgG, IgA and IgM were detected only in IV-BCG-immunized NHPs and returned to pre-vaccination levels by the time of challenge. **b**, Antibody titres in plasma ($n = 11$ –13 macaques). In plasma, both ID_{high} and IV BCG elicited increased IgG and IgA antibody responses compared to ID_{low} BCG. Data are geometric mean and s.d.; dashed line indicates assay limit of detection. A Kruskal–Wallis test was used to compare all vaccine groups to ID_{low} at weeks 4, 16 and 24 (BAL) or weeks 4 and 24 (plasma); P values are from Dunn’s multiple comparison test (colour-coded to vaccine).



Extended Data Fig. 8 | IV BCG protects against extrapulmonary disease and lung infection across a wide range of thresholds of protection.

a, Extrapulmonary disease was scored at necropsy based on a published system²⁷ taking into account the presence of *Mtb*-related pathology and *Mtb* growth from sites outside the thoracic cavity. Each symbol represents an animal and horizontal bars represent the median. Kruskal–Wallis tests were used and reported *P* values represent Dunn's multiple comparison test comparing each group to ID_{low}. All data points within the grey areas are zero.

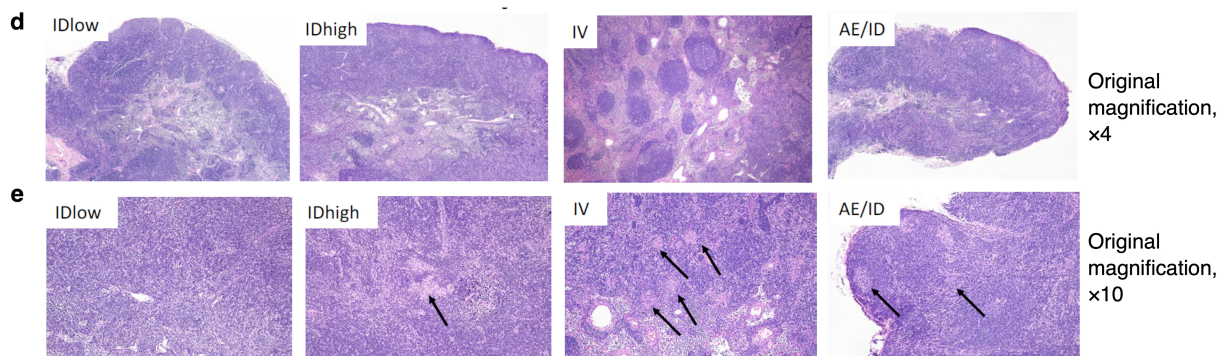
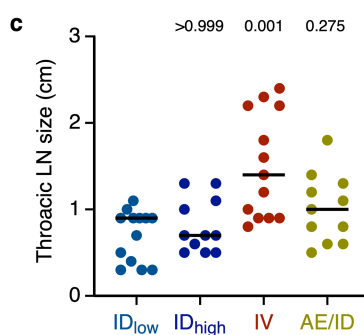
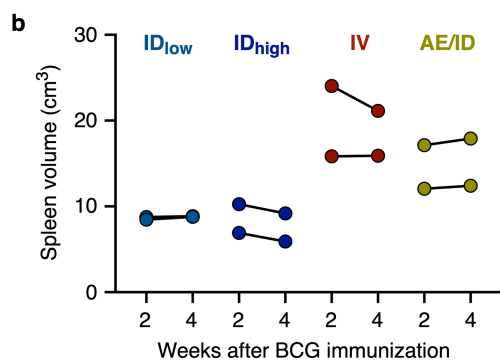
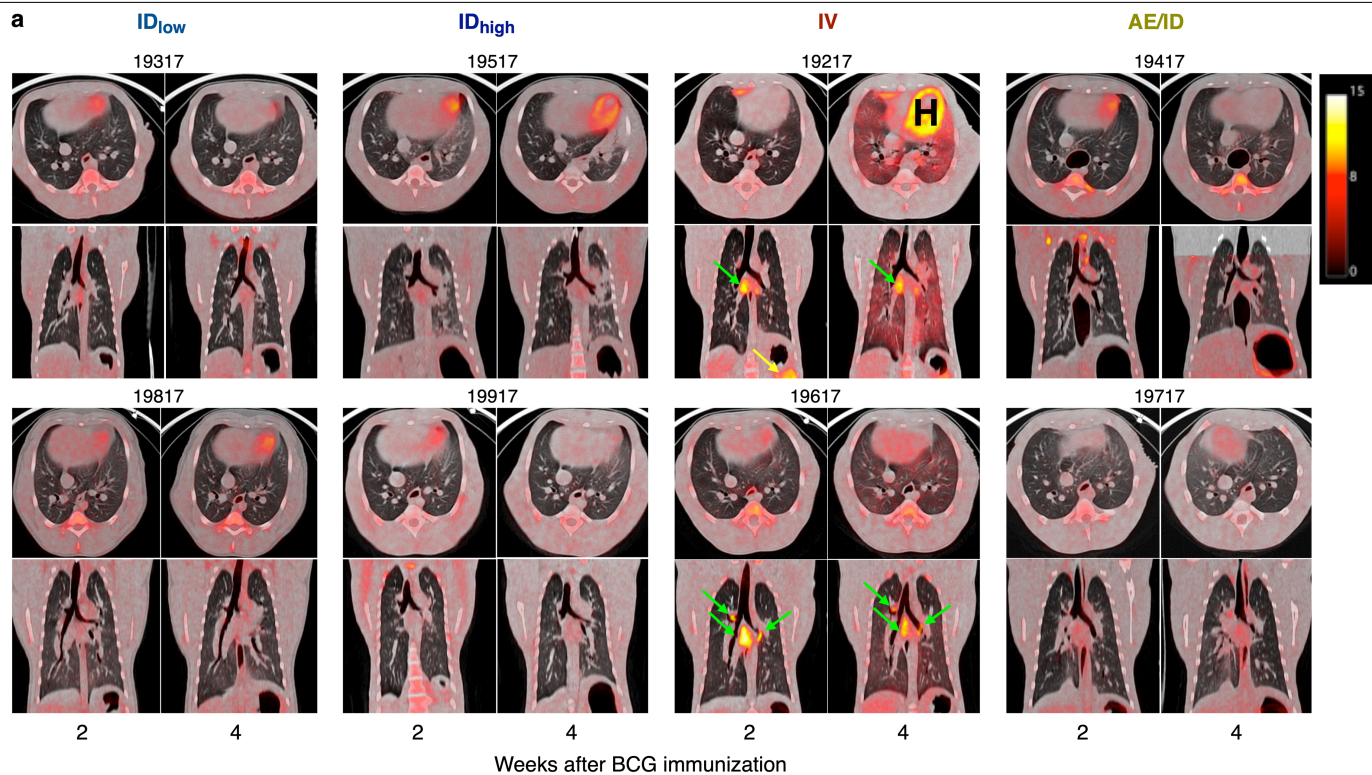
There was no extrapulmonary disease in any of the IV-BCG-vaccinated macaques, whereas the other groups had variable extrapulmonary involvement. **b**, Fisher's exact test *P* values are plotted for a range of CFU thresholds evaluating protection. For each threshold, a stacked bar plot indicates the percentage of NHPs with fewer CFUs than the threshold (that is, protected), in each vaccine group. Immunization route significantly ($P < 10^{-4}$) impacted protection at any given CFU threshold between <1 (sterile) and <10⁴.



Extended Data Fig. 9 | See next page for caption.

Extended Data Fig. 9 | Post-challenge immune responses to mycobacterial antigens. a, PBMC response to ESAT-6 or CFP-10 peptides (antigens present in Mtb but not BCG) as determined by IFN γ ELISpot throughout Mtb infection. Each line is one NHP over time ($n = 8-10$ macaques; $n = 4$ unvaccinated); sterile animals are represented by a triangle, and non-sterile, protected animals (with $1 \leq \text{CFUs} \leq 50$) denoted by squares. After infection, most animals in the AE or ID vaccine groups developed ESAT-6 or CFP10 ELISpot responses, which reflects a primary response to Mtb. By contrast, responses in the IV BCG group were lower than in the ID_{low} group at every time point after infection for ESAT-6 (4 weeks, $P = 0.001$; 6 weeks, $P = 0.045$; 8 weeks, $P = 0.025$; 12 weeks, $P = 0.006$) and CFP-10 (4 weeks, $P < 0.0001$; 6 weeks, $P = 0.035$; 8 weeks, $P = 0.001$; 12 weeks, $P = 0.004$). Kruskal-Wallis test was run at each time point with Dunn's adjusted P values reported accounting for comparisons of all groups against ID_{low}. **b, c,** The frequency of memory CD4 (**b**) and CD8 (**c**) T cells in PBMCs from

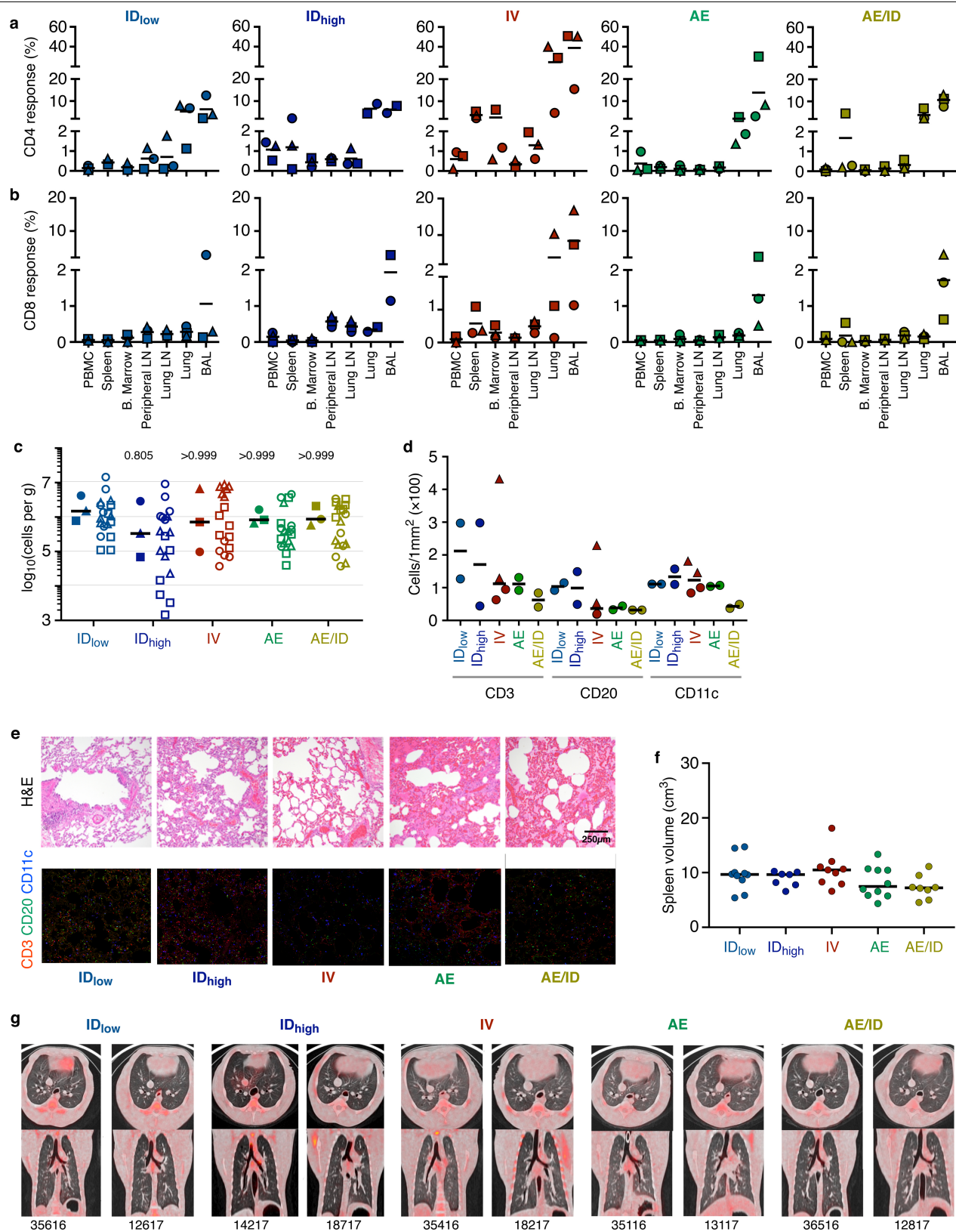
BCG-immunized NHPs ($n = 8-10$) producing any combination of IFN γ , IL-2, TNF or IL-17 in response to stimulation with either PPD (antigen present in BCG and Mtb; top row) or pooled ESAT-6 and CFP-10 peptides (antigens present in Mtb only; bottom row) were measured at the time of challenge (0), and at 4, 8 and 12 weeks after Mtb challenge. Measurements from four unvaccinated, infected NHPs are included as controls (Unvax, black). Grey lines represent the responses of individual animals and bolded, coloured lines are the mean responses for each vaccine group. **d,** Antibody responses post-challenge. Mtb WCL-specific IgG, IgA and IgM antibody titres were measured in the plasma of unvaccinated ($n = 4$) and vaccinated ($n = 8-10$) NHPs at the time of challenge (0), and at 4 and 12 weeks after challenge. In **b-d**, Wilcoxon signed-rank unadjusted P values compare cytokine frequencies or antibody titres at week 12 after Mtb (or necropsy) to the time of challenge (week 0) within each vaccine group.



Extended Data Fig. 10 | See next page for caption.

Extended Data Fig. 10 | Inflammation and gross and histopathological assessment after BCG vaccination. **a**, Serial FDG PET–CT scans at 2 and 4 weeks after BCG vaccination showed increased metabolism (surrogate for inflammation) localized to the lung LNs (green arrows), lung lobes and spleen (yellow arrow) elicited by the IV but not by other routes (cohort 5a, b, $n = 2$ macaques). Warm colours indicate increased FDG retention; scale represents standardized uptake values. NHP ID numbers are listed above each scan; ‘H’ denotes the heart. **b**, Spleen volume was calculated from CT scans at 2 and 4 weeks after BCG vaccination ($n = 2$ macaques). At these time points, animals given IV BCG had approximately twofold larger spleens than those given ID BCG, with AE/ID BCG NHPs also displaying modestly enlarged spleens. **c**, Thoracic LNs were measured at necropsy, 4 weeks after BCG vaccination ($n = 2$ macaques); LNs from IV BCG NHPs were enlarged compared to those from ID_{low} NHPs. Kruskal–Wallis test was run; Dunn’s adjusted P values are reported

comparing each vaccine group to the ID_{low} group. **d**, **e**, H&E-stained sections of thoracic LNs from vaccinated NHPs ($n = 2$ macaques), 4 weeks after BCG vaccination. **d**, General structure with respect to cortical and medullary architecture and appearance was normal in LNs from ID_{low}, ID_{high} and AE/ID vaccinated NHPs. The thoracic LNs from the IV-vaccinated macaques demonstrated marked follicular lymphoid hyperplasia, with enlarged, prominent, variably sized follicles, often with active, expanded germinal centres. Original magnification, $\times 4$. **e**, Small, non-necrotizing epithelioid histiocytic aggregates (non-necrotizing granulomas, black arrows) were abundantly disseminated within thoracic LNs from the IV BCG macaques. In the AE/ID NHPs, a wide nodal distribution of such lesions was also seen, although granuloma numbers and density were substantially less. The ID_{high} NHPs had only one observable granuloma in a single thoracic LN and in the ID_{low} NHPs, no such structures were evident. Original magnification, $\times 10$.

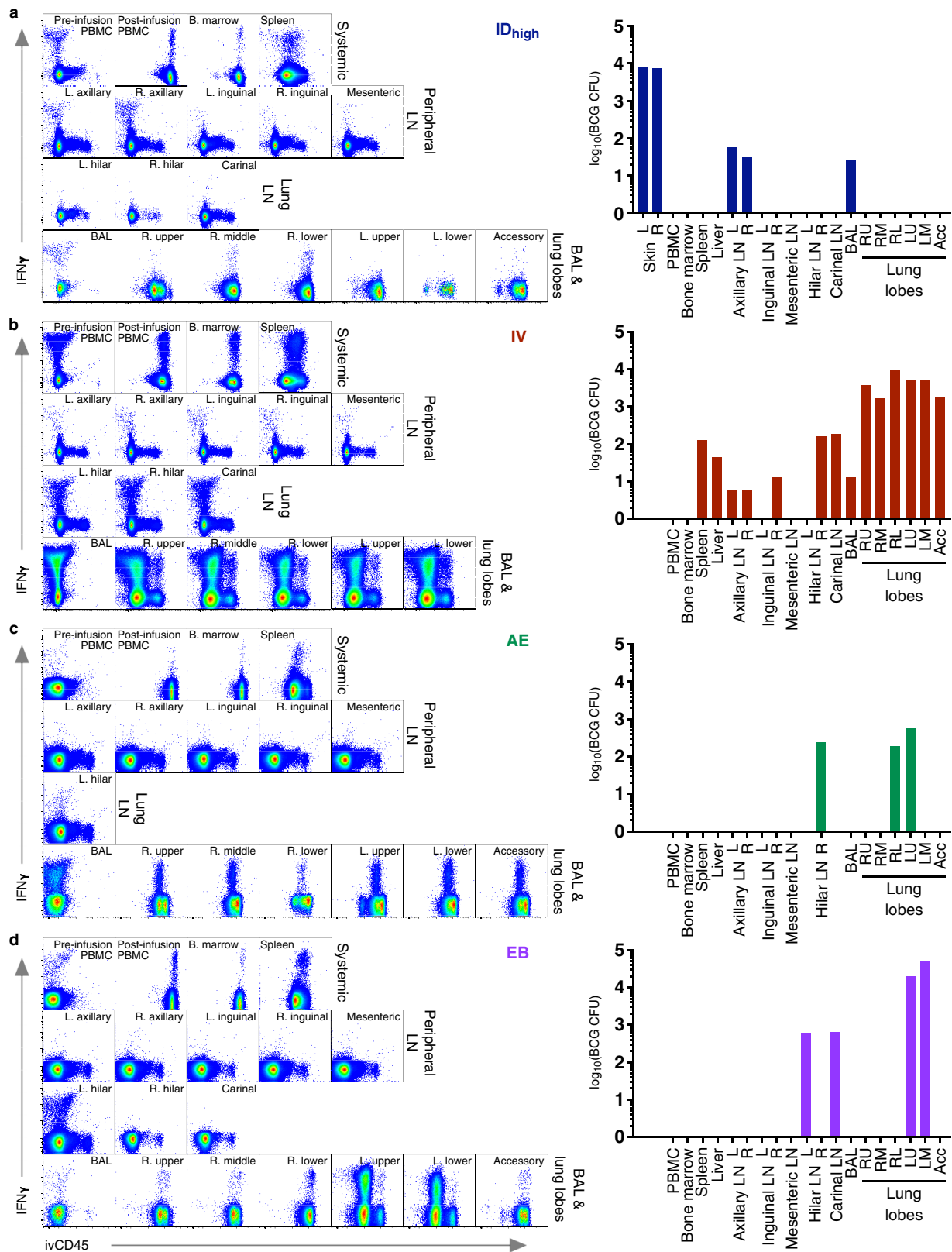


Extended Data Fig. 11 | See next page for caption.

Extended Data Fig. 11 | Immune response to BCG 6 months after vaccination.

Analysis of tissue T cell responses, lung cell counts, immunohistochemistry, splenic volume and PET-CT scans was performed 6 months after BCG vaccination. **a–c**, A separate cohort (cohort 3, $n = 3$ macaques) was vaccinated with BCG in parallel to the challenge study with the purpose of assessing immune responses in various tissues 6 months after BCG (the time point at which macaques would be challenged). **a**, **b**, Frequency of memory CD4 (**a**) and CD8 (**b**) T cells producing any combination of IFN γ , IL-2, TNF, or IL-17 in response to Mtb WCL stimulation in the PBMC, spleen, bone marrow, peripheral LN, lung LN, lung tissue and BAL. Six months after IV BCG, immunized NHPs maintained increased frequencies of antigen-responsive T cells in spleen, BAL and lung lobes. Individual LN and lung lobe responses were averaged per macaque. Data points are individual macaques with symbols matched across tissues within a vaccine group; horizontal bar indicates the mean response. **c**, Number of cells recovered per gram of lung tissue for each NHP; the increased numbers of total cells observed at 1 month post-BCG (Fig. 3d) were not detected at 6 months post-BCG. Data are shown as the median of 3 macaques per group (solid symbols, counts from six lung lobes per animal are averaged) or as counts for individual lung lobes for each animal

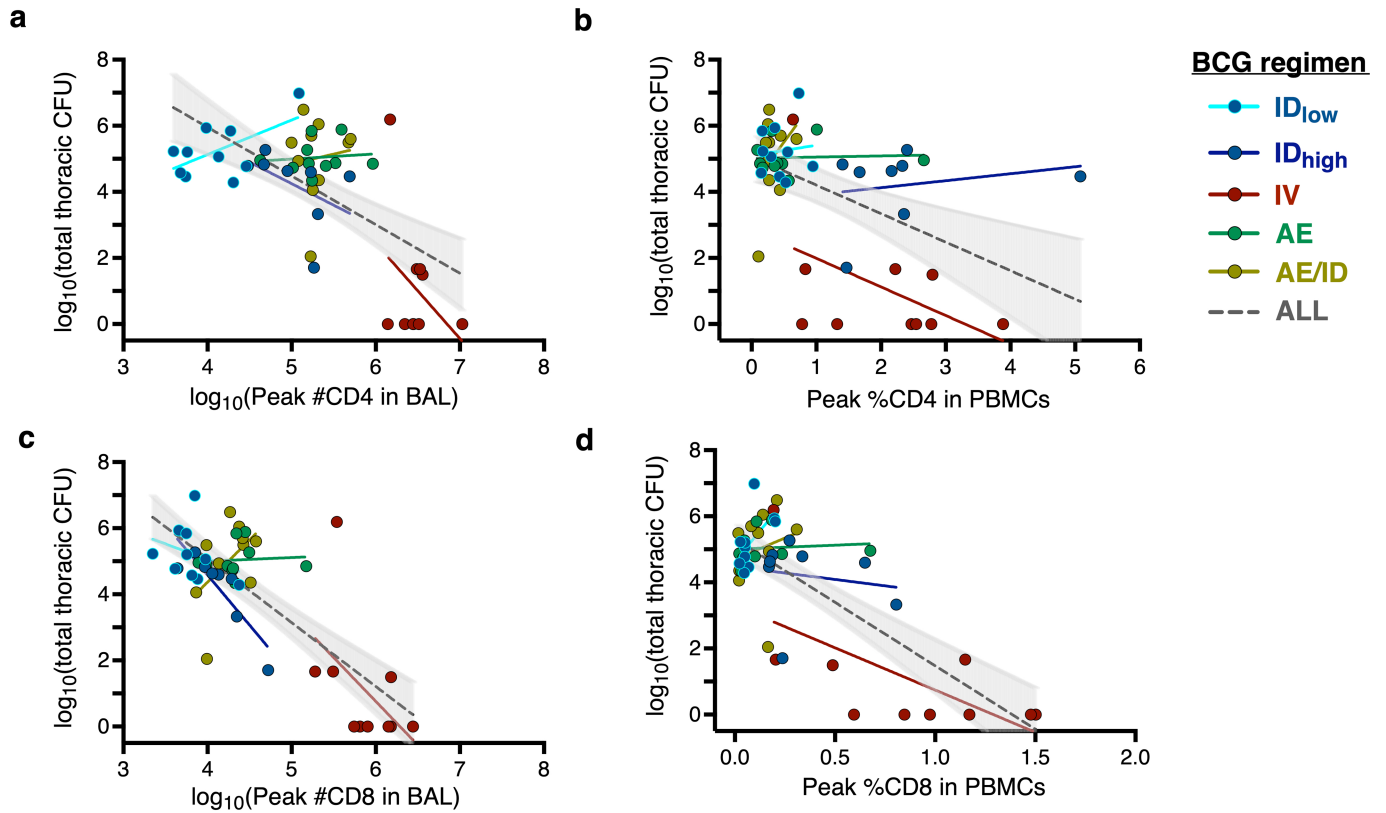
(open symbols; lobes from the same animal have matched symbols). Kruskal–Wallis test was used, and P values represent Dunn's multiple comparison test comparing each vaccine group to the ID_{low} group. **d**, Quantification of CD3⁺, CD20⁺, CD11c⁺ cells from two lung sections (matched symbols) from 1–2 macaques per group using Cell Profiler. **e**, Representative 1-mm² lung sections from 1–2 macaques per vaccine group were stained with H&E or with antibodies against CD3⁺ T cells (red), CD20⁺ B cells (green), and CD11c⁺ macrophages or dendritic cells (blue). Neither the increase in numbers of T cells and CD11c⁺ cells nor the histopathological changes in lung sections from IV-BCG-immunized macaques observed at 1 month (Fig. 3e, f) were detected 6 months after BCG vaccination. **f**, Spleen volume was calculated from CT scans of 44 NHPs (cohorts 1–3) just before Mtb challenge (6 months after BCG vaccination) and was not significantly different among vaccine routes (Kruskal–Wallis test, $P = 0.1643$). Dots represent individual animals. **g**, Axial (top) and coronal (bottom) PET–CT scans of two representative macaques ($n = 8–10$) from each vaccine group 6 months after BCG, before Mtb infection. Animal ID numbers are shown below each set of scans. No detectable lung inflammation (FDG uptake) was observed in macaques from any vaccine group.



Extended Data Fig. 12 | See next page for caption.

Extended Data Fig. 12 | Determination of immune responses and BCG in tissues 1 month after immunization. NHPs (cohort 6, $n = 2$) were immunized with 5×10^7 BCG CFUs (ID_{high} (a), IV (b), AE (c), or EB (d)); BCG CFUs and antigen-responsive T cells were measured in various tissues 1 month later. Before euthanasia, a fluorochrome-conjugated anti-CD45 antibody was injected intravenously (ivCD45) such that circulating (intravascular) leukocytes were uniformly stained (ivCD45⁺) while leukocytes in the tissue remained protected from staining (ivCD45⁻). To investigate whether antigen-responsive (IFN γ) CD4 T cells were located in the ivCD45⁻ lung tissue compartment, cells isolated

from lung lobes were re-stimulated in vitro with Mtb WCL and analysed by intracellular cytokine staining. FACS plots show memory CD4 T cells in all tissues collected from one of two NHPs per BCG regimen, organized by type/location (systemic, peripheral LN, lung LN, BAL and lung lobes). The BAL and lung responses from the IV BCG NHPs, shown in the bottom row of b, is reproduced from Fig. 4b. Pre-infusion PBMC indicates PBMCs isolated from whole blood collected just before anti-CD45 injection. Bar graphs show the number of BCG CFUs in each respective tissue for each animal (colour-coded by vaccine), if detected.



Extended Data Fig. 13 | Relationships between peak T cell responses in BAL or PBMCs and total CFUs at necropsy. a–d, Linear regressions were used to test whether antigen-responsive CD4 (a, b) or CD8 (c, d) T cell numbers (BAL; a, c) or frequencies (PBMC; b, d) after BCG immunization are associated with disease severity (total CFUs). Results indicate that when controlling for all vaccine routes, peak CD4 T cells in the BAL and PBMC, and peak CD8 T cells in

the BAL do not have a significant association with total CFUs (Supplementary Table 5a–c). Of note, in PBMCs, higher peak CD8 frequencies are associated with lower total CFUs after controlling for route (Supplementary Table 5d). Each dot represents an individual animal; coloured lines represent linear fit for each vaccine route. Dotted black lines represent linear fit for all vaccine routes combined (with 95% confidence interval shaded in grey).

Reporting Summary

Nature Research wishes to improve the reproducibility of the work that we publish. This form provides structure for consistency and transparency in reporting. For further information on Nature Research policies, see [Authors & Referees](#) and the [Editorial Policy Checklist](#).

Statistics

For all statistical analyses, confirm that the following items are present in the figure legend, table legend, main text, or Methods section.

n/a Confirmed

- ☐ ☒ The exact sample size (n) for each experimental group/condition, given as a discrete number and unit of measurement
- ☐ ☒ A statement on whether measurements were taken from distinct samples or whether the same sample was measured repeatedly
- ☐ ☒ The statistical test(s) used AND whether they are one- or two-sided
Only common tests should be described solely by name; describe more complex techniques in the Methods section.
- ☐ ☒ A description of all covariates tested
- ☐ ☒ A description of any assumptions or corrections, such as tests of normality and adjustment for multiple comparisons
- ☐ ☒ A full description of the statistical parameters including central tendency (e.g. means) or other basic estimates (e.g. regression coefficient) AND variation (e.g. standard deviation) or associated estimates of uncertainty (e.g. confidence intervals)
- ☐ ☒ For null hypothesis testing, the test statistic (e.g. F , t , r) with confidence intervals, effect sizes, degrees of freedom and P value noted
Give P values as exact values whenever suitable.
- ☒ ☐ For Bayesian analysis, information on the choice of priors and Markov chain Monte Carlo settings
- ☒ ☐ For hierarchical and complex designs, identification of the appropriate level for tests and full reporting of outcomes
- ☐ ☒ Estimates of effect sizes (e.g. Cohen's d , Pearson's r), indicating how they were calculated

Our web collection on [statistics for biologists](#) contains articles on many of the points above.

Software and code

Policy information about [availability of computer code](#)

Data collection

DiVa v7; OsiriX MD v.10.0.1

Data analysis

FlowJo v9.9.6; JMP v13; Prism v6, Excel v16.25, Pestle v1.6; SPICE v5.0; R

For manuscripts utilizing custom algorithms or software that are central to the research but not yet described in published literature, software must be made available to editors/reviewers. We strongly encourage code deposition in a community repository (e.g. GitHub). See the Nature Research [guidelines for submitting code & software](#) for further information.

Data

Policy information about [availability of data](#)

All manuscripts must include a [data availability statement](#). This statement should provide the following information, where applicable:

- Accession codes, unique identifiers, or web links for publicly available datasets
- A list of figures that have associated raw data
- A description of any restrictions on data availability

See Mss Lines 825-835

Field-specific reporting

Please select the one below that is the best fit for your research. If you are not sure, read the appropriate sections before making your selection.

- ☒ Life sciences ☐ Behavioural & social sciences ☐ Ecological, evolutionary & environmental sciences

For a reference copy of the document with all sections, see [nature.com/documents/nr-reporting-summary-flat.pdf](https://www.nature.com/documents/nr-reporting-summary-flat.pdf)

Life sciences study design

All studies must disclose on these points even when the disclosure is negative.

Sample size	See Mss Lines 869-880 (M&M, "Animals")
Data exclusions	No data excluded
Replication	See Extended Data Figure 1
Randomization	See Mss Lines 883-885 (M&M "BCG Vaccination")
Blinding	Pathologists performing the necropsies, analysts reading PET-CT scans, and technicians processing tissues were blinded from treatment group

Reporting for specific materials, systems and methods

We require information from authors about some types of materials, experimental systems and methods used in many studies. Here, indicate whether each material, system or method listed is relevant to your study. If you are not sure if a list item applies to your research, read the appropriate section before selecting a response.

Materials & experimental systems

n/a	Involved in the study
<input type="checkbox"/>	<input checked="" type="checkbox"/> Antibodies
<input checked="" type="checkbox"/>	<input type="checkbox"/> Eukaryotic cell lines
<input checked="" type="checkbox"/>	<input type="checkbox"/> Palaeontology
<input type="checkbox"/>	<input checked="" type="checkbox"/> Animals and other organisms
<input checked="" type="checkbox"/>	<input type="checkbox"/> Human research participants
<input checked="" type="checkbox"/>	<input type="checkbox"/> Clinical data

Methods

n/a	Involved in the study
<input checked="" type="checkbox"/>	<input type="checkbox"/> ChIP-seq
<input type="checkbox"/>	<input checked="" type="checkbox"/> Flow cytometry
<input checked="" type="checkbox"/>	<input type="checkbox"/> MRI-based neuroimaging

Antibodies

Antibodies used	See Suppl Data 8-11
Validation	All monoclonal antibodies used for flow cytometry were titrated to obtain optimal signal to noise, comparing the specific staining to a gold standard or previously published monoclonal antibody to ensure the staining is biologically appropriate.

Animals and other organisms

Policy information about [studies involving animals](#); [ARRIVE guidelines](#) recommended for reporting animal research

Laboratory animals	See Mss Lines 857-867 (M&M, "Animals")
Wild animals	N/A
Field-collected samples	N/A
Ethics oversight	See Mss Lines 857-867 (M&M, "Animals")

Note that full information on the approval of the study protocol must also be provided in the manuscript.

Flow Cytometry

Plots

Confirm that:

- ☐ The axis labels state the marker and fluorochrome used (e.g. CD4-FITC).
- ☒ The axis scales are clearly visible. Include numbers along axes only for bottom left plot of group (a 'group' is an analysis of identical markers).
- ☒ All plots are contour plots with outliers or pseudocolor plots.
- ☒ A numerical value for number of cells or percentage (with statistics) is provided.

Methodology

Sample preparation	See mss Lines 972-1002 (M&M Multiparameter Flow Cytometry)
Instrument	BD LSR II and BD Symphony A5
Software	Diva v7 and FlowJo v9.9.6
Cell population abundance	N/A
Gating strategy	See Supplemental data 8-11

☒ Tick this box to confirm that a figure exemplifying the gating strategy is provided in the Supplementary Information.